Rare Metals

WILEY | 有科出版 YOUKE PUBLISHING

MINI REVIEW OPEN ACCESS

A Mini Review on Evolution of High-Entropy Alloy Design: From Experimental Approaches to Machine Learning Integration

Chrispin Ouko Zamzu | Zhe Jia | Baolong Shen

Jiangsu Key Laboratory for Advanced Metallic Materials, School of Materials Science and Engineering, Southeast University, Nanjing, China

Correspondence: Zhe Jia (zhejia@seu.edu.cn) | Baolong Shen (blshen@seu.edu.cn)

Received: 5 August 2025 | **Revised:** 28 September 2025 | **Accepted:** 30 September 2025

Keywords: alloy design | high entropy alloys | high-throughput | machine learning | microstructure and mechanical properties

ABSTRACT

High-entropy alloys (HEAs) have emerged as a transformative class of materials distinguished by their complex chemical compositions, unique microstructures, and remarkable mechanical and functional properties. Traditionally, the discovery and optimization of HEAs have relied on conventional methods, including trial-and-error experimentation, first-principles calculations, molecular dynamics (MD), and CALculation of PHAse Diagrams (CALPHAD). Although these techniques have contributed immensely to the discovery of HEAs, they struggle to efficiently and accurately navigate the vast and complex compositional space of HEAs owing to their inherent limitations. This review presents the evolution of HEA design methodologies, with a key focus on the paradigm shift brought about by the integration of machine learning (ML) into the HEA discovery process. It unifies composition design, phase prediction, microstructure analysis, and property/process optimization within a single coherent framework. In addition, frontier developments, such as the generative adversarial network (GAN)-based data augmentation to tackle the issue of limited datasets, active learning loops for targeted experimentation, and hybrid ML-physics models that incorporate fundamental strengthening mechanisms, are emphasized. Efforts to address persistent challenges include the use of local interpretable model-agnostic explanation (LIME) and SHapley Additive exPlanations (SHAP), alongside physics-informed approaches, to improve model interpretability, whereas Bayesian-based techniques are utilized to improve uncertainty quantification. The synergy between experimental, computational, and data-driven approaches is highlighted as a key driver for creating predictive alloy-design frameworks that are both efficient and physically interpretable. By bridging conventional and data-driven approaches, this study not only deepens the understanding of HEA design principles but also outlines how emerging ML strategies are poised to accelerate the transition from material conception to application. An outlook on next-generation ML-driven HEA design is presented, with an emphasis on addressing current limitations and leveraging recent breakthroughs to expand the frontiers of material discovery.

1 | Introduction

1.1 | Background and Significance of High-Entropy Alloys (HEAs)

HEAs were first introduced in 2004 by Yeh et al. [1] and Cantor et al. [2], who worked independently on CuCoNiCrAlFe and FeCrMnNiCo alloys, respectively. Since then, multicomponent alloy systems have garnered significant attention due to their broader range of compositional designs compared with those of conventional alloys. Figure 1 illustrates the development of HEAs from experimental approaches to the integration of ML techniques. HEAs possess unique microstructures and functional properties, making them potential candidates for a wide range of functional and structural applications [8].

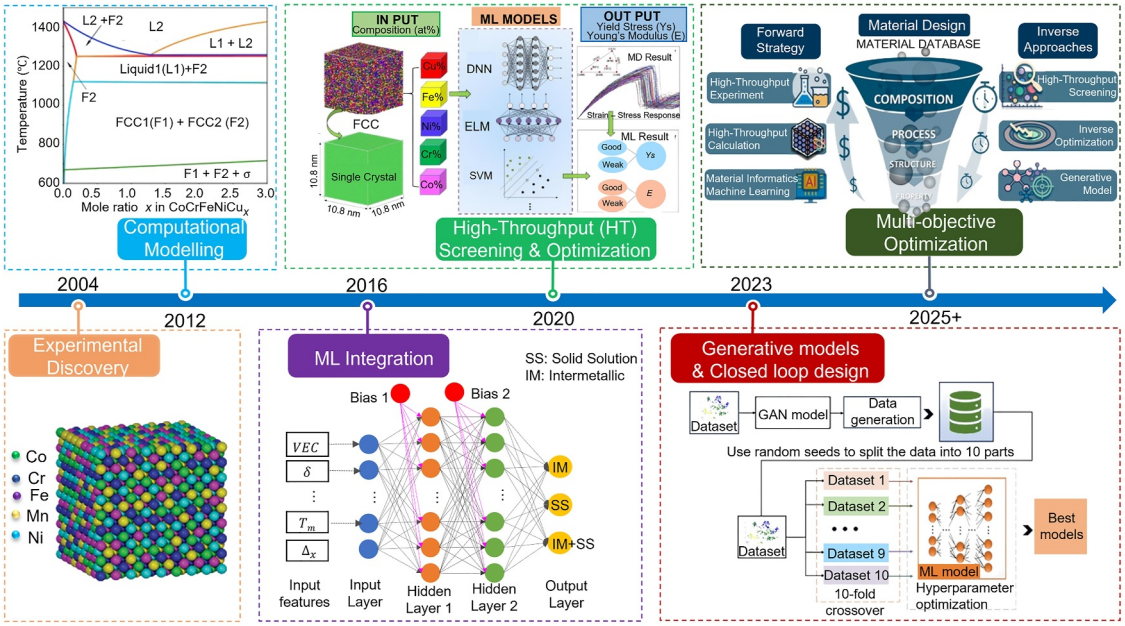

FIGURE 1 | Development of HEAs from experimental to ML integration. The figure illustrates the evolving design process of HEAs, beginning with classical methods such as trial-and-error and experimental testing, progressing through computational models, and culminating in the adoption of ML to predict material properties, optimize compositions, and accelerate the discovery of new alloys [3–7].

1.1.1 | Definition and Core Characteristics of HEAs

The term HEAs was coined by Yeh et al. [9], whereas Cantor et al. [2] used the term multicomponent alloys to refer to alloys containing multiple elements in near-equiatomic concentrations. Based on their composition, HEAs are alloys consisting of multiprincipal element compositions (at least five elements), with atomic percentages ranging from 5% to 35% [9]. Moreover, the atomic proportion of any minor element, if present, is < 5%. In contrast to the conventional view, this compositional complexity does not necessarily lead to microstructural complexities (such as compound formation) because of the influence of increased entropy. Thus, HEAs can also be defined in terms of their higher configurational entropy of mixing compared with that of conventional alloys. Based on Boltzmann's hypothesis of the relationship between entropy and system complexity, the mixing configurational entropy change for an ideal solid solution is expressed, as shown in Equation (1), where R is the gas constant, n is the number of elements, and x_i is the mole fraction of the i_{th} element [1].

$$\Delta S_{\text{mix}} = -R\sum_{i=1}^{n} x_i \ln x_i \tag{1}$$

In an equiatomic alloy, $x_1 = x_2 = x_3 = \ldots x_n$, the mixing configurational entropy per mole is expressed as Equation (2).

$$\Delta S_{\text{mix}} = -R\left(\frac{1}{n}\ln\frac{1}{n} + \frac{1}{n}\ln\frac{1}{n} + \frac{1}{n}\ln\frac{1}{n} + \ldots\frac{1}{n}\ln\frac{1}{n}\right) = -R\ln n \tag{2}$$

It is evident from Equation (2) that ΔS_{mix} increases with an increase in the number of elements in the system, that is, $0.693R$, $1.10R$, $1.386R$, and $1.61R$ for binary, ternary, quaternary, and quinary equimolar alloys, respectively. Thus, Equation (2) defines HEAs by relating the number of principal elements to the system's mixing entropy; low-entropy alloys have $\Delta S_{\text{mix}} < 0.693R$, medium-entropy alloys have $0.693R < \Delta S_{\text{mix}} < 1.61R$, and high-entropy alloys have $\Delta S_{\text{mix}} > 1.61R$ [9, 10]. However, because very few conventional alloys can have $\Delta S_{\text{mix}} > 1.5$, this boundary is often used as the operational definition of HEAs [9]. Among the factors influencing the microstructure and properties of HEAs, the "four core effects" have been identified as the most significant, as illustrated in Figure 2. These include the high-entropy effect for thermodynamics, severe lattice distortion effect for structure, cocktail effect for properties, and sluggish diffusion [9]. Other factors, such as stress, temperature, and strain rate during processing or application, also affect the microstructure and properties of HEAs.

1.1.1.1 | High-Entropy Effect. The high-entropy effect is arguably the most significant of the "four core effects" in HEAs because it promotes the formation of solid solutions. In the binary phase diagrams of conventional alloys, solid solutions are generally found at the compositional extremes, whereas ordered intermediate phases tend to form near the center of the phase diagram [11]. Thus, as the number of elements in concentrated alloys increases, the probability of some elements reacting to form compounds also increases. However, this is not the case for HEAs. HEAs in the solid-state exhibit two competing phases: intermetallic compounds and solid-solution phases. According to the second law of thermodynamics, as expressed in Equation (3), the equilibrium state is the one with the lowest Gibbs free energy (ΔG_{mix}) among all possible states at a given temperature and pressure.

$$\Delta G_{\text{mix}} = \Delta H_{\text{mix}} - T\Delta S_{\text{mix}} \tag{3}$$

where ΔH_{mix} is the enthalpy of mixing, T is the temperature, and ΔS_{mix} is the entropy of mixing.

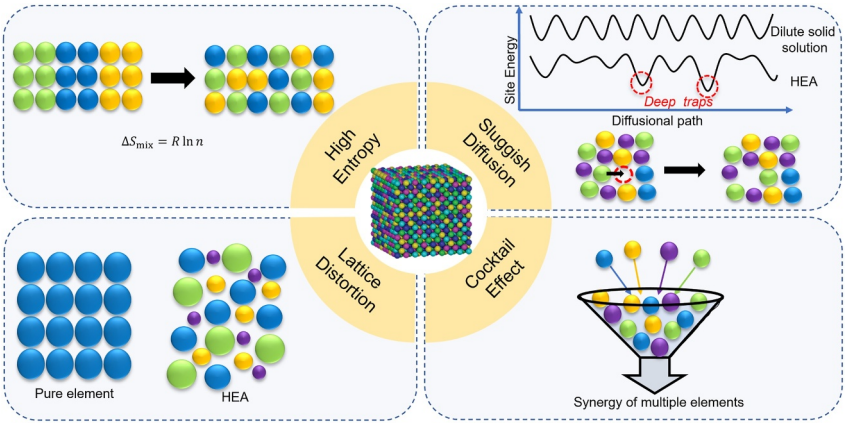

FIGURE 2 | Four core effects influencing properties of HEAs. These include the high-entropy effect, which promotes solid-solution formation; the severe lattice distortion effect, which enhances mechanical properties; the cocktail effect, which results in unique combinations of elemental properties; and sluggish diffusion, which affects the rate of atomic movement and contributes to the stability and strength of HEAs. These effects collectively define the distinct advantages of HEAs over traditional alloys.

Regardless of the atomic size difference, compound phases have large ΔH_{mix} but small ΔS_{mix}, whereas solid-solution phases containing multiple elements have medium ΔH_{mix} and high ΔS_{mix}. Yeh et al. [1] theorized that the presence of multiple elements in near-equiatomic proportions has the potential to increase ΔS_{mix} enough to overcome compound formation enthalpies, thereby preventing harmful intermetallics and stabilizing solid solutions. However, the magnitude of ΔS_{mix} in an HEA does not guarantee the suppression of intermetallic compounds, but it does increase the probability of this occurring [12, 13]. The effect of high entropy on the phase stability of solid solutions in HEAs has been validated in various studies [11, 13–17]. Although the high entropy of mixing plays a key role in the stability of solid-solution phases, Otto et al. [13] and Yang et al. [18] noted that, by itself, it is generally unable to override competing driving forces, such as enthalpy and nonconfigurational entropy, which also govern phase stability. Nonconfiguration entropy arises from vibrational, electronic, and magnetic effects.

1.1.1.2 | Sluggish Diffusion. During phase transformation, the nucleation and growth of new phases require the cooperative diffusion of multiple types of atoms in HEAs to achieve compositional partitioning. This, combined with the distorted lattice, results in a slow diffusion rate in HEAs [19]. Despite the complex atomic environment in HEAs, vacancy formation is governed by fundamental thermodynamic principles similar to those governing vacancy formation in conventional alloys. The balance between the vacancy formation energy and entropy effects dictates the equilibrium vacancy concentration, preventing the formation of an unlimited number of vacancies. Moreover, unlike in conventional alloys, where vacancies primarily interact with one type of solute, in HEAs, vacancies interact with a diverse mix of elements, influencing the diffusion rates and pathways in a more complex manner. Tsai et al. [20] employed the diffusion couple method to investigate the diffusion parameters of Co, Cr, Fe, Mn, and Ni in an ideal solution-like CoCrFeMnNi alloy, revealing lower diffusion coefficients and higher activation energies compared to those of conventional FCC metals. The theory of sluggish diffusion was also confirmed by Dabrowa et al. [21], who conducted an interdiffusion experimental study on CoCrFeMnNi and AlCoCrFeNi HEAs. The mechanism for sluggish diffusion in HEAs is related to fluctuations in lattice potential energy (LPE), which create an uneven atomic environment, leading to higher activation energy barriers for atomic migration and trapping of atoms in low-LPE sites, further hindering their movement [19, 22]. Thomas and Patal [22] also pointed out that diffusion in HEAs can be tuned and is not inherently sluggish, with factors beyond migration barriers also influencing diffusion behavior. The slower diffusion rates and phase transformation kinetics of HEAs play a significant role in enhancing their microstructural stability and mechanical performance.

1.1.1.3 | Severe Distortion Effect. Severe lattice distortion in HEAs results from the presence of multiple principal elements, where diverse neighboring atoms surround each atom. The severity of lattice distortion is influenced by factors such as atomic size differences, bonding characteristics, and electronic structures of the constituent elements [19, 23]. Variations in atomic size cause larger atoms to displace neighboring atoms outward, whereas smaller atoms generate voids or regions with lower atomic density. The bonding and electronic structures between an atom and its nearest neighbors are asymmetric, and this asymmetry varies from lattice site to lattice site. Cheng et al. [19] studied Ni, NiCo, NiCoFe, NiCoFeCr, and NiCoFeCrMn alloys, demonstrating that the addition of elements resulted in greater lattice distortion (up to 1.4% in NiCoFeCrMn), lower melting points, decreased thermal conductivity, and reduced X-ray peak intensity due to enhanced diffuse scattering. Severe lattice distortion influences mechanical properties, such as strength, ductility, Young's modulus, and hardness [24]. In pure metals, dislocations move smoothly, whereas, in dilute solutions, they are partially hindered by solute atoms. In concentrated solutions, dislocation lines are significantly dragged by solutes, forming serrated patterns.

1.1.1.4 | Cocktail Effect. The term cocktail effect refers to the combined influence of the composition, structure, and microstructure of HEAs. The comprehensive properties of HEAs arise from the intrinsic properties of the elements, as predicted by the rule of mixtures, complex interactions, and severe lattice distortion. The “cocktail effect” emphasizes that unique material

properties often emerge from unexpected synergies. Therefore, understanding the key influencing factors is essential when selecting an appropriate composition and processing method. Refractory high-entropy alloys (RHEAs) such as NbMoTaW and VNbMoTa leverage the cocktail effect by incorporating high-melting point elements, resulting in significantly higher melting points than those of Ni- and Co-based superalloys [25, 26]. This enhances their high-temperature strength, surpassing that of conventional superalloys, making them promising candidates for applications at extreme temperatures. Other mechanical properties, including wear and corrosion resistance, can be improved by deliberately incorporating elements known for their high wear and corrosion resistance [27]. Cocktail alloying can also embed metastable crystalline structures within HEAs, contributing to strengthening through transformation-induced plasticity (TRIP) and twinning-induced plasticity (TWIP) effects [28]. The enhanced strain-hardening capacity results from dislocation hardening in the stable phase, whereas the TRIP and TWIP of the metastable phase lead to improved ductility [29–32].

1.1.2 | Properties and Potential Applications of HEAs

The properties of materials are significantly influenced by factors such as composition, microstructure, and processing routes, with the intrinsic correlation between microstructural heterogeneity and functional performance playing a crucial role [33]. The phases present in HEAs can include solid solutions (such as FCC, BCC, or HCP), intermetallic, amorphous phases, or a combination of these. Adjusting the microstructure from one phase to another or even to a multiphase state can be accomplished by incorporating elements such as Al, V, Cr, Mo, and Si [14, 34–37]. FCC single-phase HEAs, which are primarily composed of Cr, Co, Fe, Ni, Mn, and Cu, are known for their high ductility [38, 39] and high fracture toughness [40–42] but tend to have relatively low ultimate tensile strength, yield strength, and hardness [43]. BCC HEAs are classified into two categories: those consisting of Cr, Co, Fe, Ni, Mn, and Cu, and those made up of refractory elements such as V, Cr, Ti, Mo, Nb, Ta, W, Zr, and Hf [44]. BCC HEAs, such as AlCoCrFeNiV [45], AlCoCrCuFeNi [46], and AlCoCrFeNi [47], typically exhibit both high hardness and compressive strength but low ductility. RHEAs are notable for their exceptional high-temperature strength, as observed in TaNbHfZrTi [48] and NbMoTaWZr [49], as well as high-temperature oxidation resistance, as demonstrated by MoWAlCrTi [50]. Considerable efforts have focused on resolving the strength–ductility trade-off in RHEAs, aiming to optimize their mechanical performance for demanding applications [51–53]. Conversely, multiphase HEAs exhibit an excellent combination of strength and ductility, which is often a challenge for single-phase HEAs. These multiphase HEAs include dual-phase FCC + BCC [34, 35, 37, 45], dual-phase FCC + intermetallic (IM) [45, 54, 55], dual-phase BCC + IM [45, 56], and triple-phase FCC + BCC + IM [57, 58]. The AlCoCrCuFeNi alloy system has been extensively researched due to its dual-phase structure (FCC + BCC), which significantly influences its properties [34, 35, 37, 45]. Additionally, nonmetallic elements such as C, Si, N, and O have been utilized to enhance the mechanical properties of $(Al_{0.3}CoCrFeNi)Si_x$ [36], $(NbMoTaW)Si_2$ [59, 60], $(Fe_{40}Mn_{40}Co_{10}Cr_{10})C_x$ [61], $(NbZrTi)O_x$ [62], and $NbMoTaW(HfN)_x$ HEAs [63]. Interstitial elements such as C, B, N, O, and H influence the microstructure, thermal stability, mechanical properties, and deformation behavior of HEAs [64].

Because of their remarkable combination of properties, HEAs are emerging as potential candidates for a range of high-performance applications across different sectors [65]. In the aerospace industry, refractory HEAs such as MoNbTaW, MoWAlCrTi, and MoNbTaVW offer superior high-temperature strength and oxidation resistance compared to conventional alloys, making them ideal for applications within the engine environment above 1273 K [50, 66]. The presence of Al and Cr contributes to the formation of stable oxide layers, further enhancing corrosion resistance. Kuang et al. [59] demonstrated the excellent oxidation resistance of the high-entropy refractory metal silicide $(NbMoTaW)Si_2$ coating, which performed exceptionally well in an atmospheric environment at 1573 K. Yttrium-modified $(NbMoTaW)Si_2$ coating has also been demonstrated to exhibit exceptional antiablation performance in an oxidizing environment at 2373 K for 180 s, displaying negligible signs of ablation damage [60]. Moreover, one of the dominant failure modes at high temperatures is thermal creep. Therefore, the design of RHEAs requires an understanding of how their microstructure, local chemical distribution, atomic movement modes, and deformation mechanisms affect creep behavior [67, 68]. Exceptional high-temperature creep resistance, comparable to that of single-crystal Ni-based superalloys, has been observed in $Ta_{27.3}Mo_{27.3}Ti_{27.3}Cr_8Al_{10}$ RHEA with a stable A2+B2 microstructure. This was attributed to effective precipitate strengthening and directional coarsening driven by lattice misfit. In the defense sector, HEAs are considered potential materials for armor and ballistic protection due to their high hardness, toughness, and wear resistance. CoCrFeNiTi, AlCoCrFeNiV, AlCoCrFeNiSc, and AlCoCrCuFeNi HEAs have demonstrated exceptionally high hardness values exceeding 600 HV [43, 46, 69], and $Al_{0.1}CoCrFeNi$ boasts a high impact resistance of 400 J [41], making them suitable for armor plating applications. HEAs are also being considered for use in the nuclear industry because of their outstanding radiation resistance. Structural materials used in nuclear components, such as reactors, are subjected to harsh conditions characterized by high temperatures and radiation doses. The irradiation resistance of FeMnCrVAlC [70], AlCoCrFeNi, CrMnFeCoNi, $Ti_2ZrHfV_{0.5}Mo_{0.2}$, and $W_{38}Ta_{36}Cr_{15}V_{11}$ [8] has attracted significant attention. For instance, FeMnCrVAlC showed no signs of irradiation hardening when exposed to 1 displacement per atom (dpa) at 573 and 773 K [59]. AlCoCrFeNi maintained excellent structural stability when irradiated to over 50 dpa at 298 K [8]. The sluggish diffusion characteristics slow atomic movement, reducing radiation-induced void swelling and preventing material degradation over time. The complex atomic arrangement from lattice distortion disrupts defect formation and migration, enhancing resistance to radiation-induced embrittlement.

The composition of HEAs can be tuned for catalytic applications by incorporating catalytically active elements [71]. The multielement nature of HEAs results in a synergistic effect that boosts their catalytic activity, stability, and selectivity compared to conventional single-element catalysts. Examples of HEA catalysts and processes in which they have been evaluated include PtPdRhRuCe [72] and CoMoFeNiCu [73] for ammonia decomposition; AuAgPtPdCu for the reduction of carbon dioxide (CO_2)

and carbon monoxide (CO) [74]; FeCoNiAlTi [75]; TiVCrMnMoCe [76]; AlFeCoNiMo [77]; $Fe_{10}Co_5Ni_{10}Cu_{15}Al_{60}$ [78]; and FeCoNiCrPt [79] for hydrogen generation. Alloys based on HEAs demonstrate higher efficiency and enhanced durability, with minimal loss of catalytic activity during extended use. For instance, PtPdRhRuCe catalysts achieved ~100% ammonia conversion and more than 99% nitrogen oxide selectivity during extended operations (~30 h) at relatively low temperatures (973 K) [72]. Moreover, the discovery of chemical short-range order in low-cost $Fe_{10}Co_5Ni_{10}Cu_{15}Al_{60}$ HEAs, influenced by magnetic interactions, resulted in a remarkable improvement in water splitting efficiency, achieving a current density of 130 mA cm^{-2}, which is nearly four times greater than that of the Pt/C||RuO_2 system [78].

In addition to crystalline HEAs, their amorphous counterparts, high-entropy metallic glasses (HEMGs), have also garnered attention for their potential in catalytic applications. Metallic glasses, although macroscopically homogeneous due to the absence of typical defects such as grain boundaries and vacancies, exhibit intricate local structural heterogeneities with significant dynamical and spatial variations [80]. Characterized by their disordered atomic structure, multicomponent composition, and broad elemental miscibility, HEMGs exhibit unique catalytic properties similar to those of traditional metallic glasses [81–89]. Notably, HEMGs such as PdPtCuNiP [90], $(FeCoNiB_{0.75})_{97}Pt_3$ [91], and PtPdNiP [92] have demonstrated ultralow overpotentials for the hydrogen evolution reaction (HER) and oxygen evolution reaction (OER). Zhang et al. [91] defect-engineered $(FeCoNiB_{0.75})_{97}Pt_3$ HEMG with only 3 at% Pt, resulting in a cost-effective electrocatalyst with abundant active sites due to lattice distortions and stacking faults induced by boron. The catalyst exhibited ultralow overpotentials for HER of 104 mV and OER of 301 mV at 1000 mA cm^{-2} in alkaline media, with over 200 h of stability at 100 mA cm^{-2}. It also achieved HER overpotentials of just 81 and 122 mV at 1000 and 100 mA cm^{-2} under acidic and neutral conditions, respectively, outperforming commercial Pt/C and RuO_2. Additionally, amorphous FeCoNiPb-based high-entropy oxides [93, 94] and dual-phase (crystalline–amorphous) multielement alloy (PdTiZrAlCuZnNiSiO) [95] have also demonstrated excellent catalytic activity for hydrogen generation. Although not composed of high-entropy materials, recent work on single-atom Fe dispersed within amorphous Mo-based nanosheets demonstrates how atomic-scale disorder and heterointerfaces can be leveraged to enhance HER activity and durability, offering insights relevant to the catalytic design of HEAs and HEMGs [96]. HEAs are also considered promising candidates for hydrogen storage due to their unique multielement compositions, which enhance the processes of hydrogen absorption and desorption. Ti-based HEAs, such as TiZrVMoNb, TiZrHfMoNb, and NbTiVZr, undergo a phase change from BCC to FCC when hydrogen absorption reaches a specific threshold [97, 98]. In the BCC phase, hydrogen mainly occupies octahedral interstitial sites. However, in the FCC phase, as the hydrogen content increases, the preferred occupancy of hydrogen shifts from octahedral to tetrahedral sites [97]. This shift is attributed to the lattice distortion effect, which facilitates the occupation of both octahedral and tetrahedral interstitial sites by hydrogen atoms.

HEAs are ideal for use in harsh environments, such as deep-sea exploration, owing to their high mechanical strength, resistance to corrosion, and fracture toughness. These materials can withstand high pressures, extremely low temperatures, and corrosive substances. Gludovatz et al. [40] reported an FCC CrMnFeCoNi alloy that demonstrated remarkable fracture toughness and tensile strengths exceeding 200 MPa$\sqrt{m}$ and 1000 MPa, respectively, at cryogenic temperatures as low as 77 K. Unlike conventional alloys that experience low-temperature embrittlement, this alloy exhibits a simultaneous improvement in both strength and ductility as the temperature decreases. Wetzel et al. [99] compared the corrosion behaviors of CrMnFeCoNi, CrCoN, and AISI 304 stainless steels in H_2SO_4 and NaCl aqueous solutions. CrCoN exhibited superior corrosion resistance in both solutions, whereas CrMnFeCoNi was susceptible to pitting corrosion in the NaCl solution. Additionally, AlCoCrFeNi has been reported to show an exceptional combination of mechanical, wear-resistant, and corrosion-resistant properties compared to 2205 duplex stainless steel (DSS) and Incoloy 825 alloys [100]. Because of their excellent biocompatibility, antimicrobial property, and resistance to corrosion compared to stainless steel and Ti, HEAs such as $CrFeNi_{0.5}Cu_{0.3}$ [101], TiZrNbTa [102], TiNbTaZrMo, and TiZrHfNbTaMo [103] are promising for use in medical implants and surgical tools. The tunable magnetic properties of HEAs, such as AlCoCrFeNi [46], $FeCoNi(CuAl)_{0.8}$ [104], FeCoNiPd, and FeCoNiPt [105], make them suitable for developing soft magnets used in advanced magnetic recording and data storage, inductors, and magnetic sensors.

1.2 | Conventional Experimental Methods

Experimentation remains one of the most effective methods for discovering new alloys. Methods such as arc melting, induction melting, and powder metallurgy are widely used for HEA synthesis [106]. X-ray diffraction (XRD), scanning electron microscopy (SEM), energy-dispersive X-ray spectroscopy (EDS), and transmission electron microscopy (TEM) are commonly employed to characterize their microstructure, whereas mechanical tests such as tensile tests and hardness tests are used to assess their mechanical properties [26, 39]. These techniques provide direct insights into the synthesis–microstructure–properties relationship in HEAs. However, the concept of HEAs has significantly broadened the range of potential compositions, making it impractical to explore them all using these techniques, which are often time-consuming and resource-intensive. Furthermore, conventional methods are limited in their ability to guide alloy design without extensive trial-and-error experimentation. These methods are increasingly being complemented by high-throughput and computational approaches to accelerate HEA design [107, 108]. These approaches allow the exploration and prediction of HEA compositions and properties before significant investments in experimental processes are made.

1.3 | Combinatorial Synthesis

Combinatorial synthesis involves the rapid creation of a wide range of alloy composition gradients using techniques such as rapid alloy prototyping [109], diffusion multiples [109–111], laser additive manufacturing [112, 113], and multitarget cosputtering [109, 114]. The first four techniques are used for composition-graded bulk alloys, whereas the latter is used for thin films.

Rapid alloy prototyping combines casting, rolling, and heat treatment of multiple alloys with specific compositions, followed by analyses of their microstructures and properties [109]. However, it is constrained by the number of alloy compositions, which is typically around five in one processing run. Diffusion multiples are an extension of diffusion couples, in which three or more components are placed in diffusional contact, enabling the collection of data for ternary and more complex systems [109–111]. This method enables the efficient exploration of composition–structure–property relationships across various phases, providing a faster alternative to traditional methods that examine one composition at a time. Characterization is typically performed using localized techniques such as electron probe microanalysis, EBSD, nanoindentation, atomic force microscopy, and microscale thermal analysis [109]. Although the cost of creating samples for diffusion multiples is relatively low, the process requires extended heat treatment at high temperatures, often around 1200°C for over 24 h, to achieve the desired diffusion gradients [110, 111]. Additionally, characterization techniques are generally confined to small local areas, usually at the microscale.

Laser additive manufacturing techniques, such as laser-engineered net shaping (LENS), have also been employed to prepare compositionally graded HEAs [112, 113]. These systems can be equipped with four or more feedstock nozzles, allowing the delivery of powders with varying compositions to the laser, thereby enabling the creation of virtually unlimited compositional gradients in the material. Additive manufacturing enables the fabrication of bulk alloys that are difficult to produce via conventional casting; however, the process can be costly because of the requirement for large quantities of prealloyed powders. Combinatorial direct-current magnetron sputtering is another versatile method for synthesizing compositionally graded HEA films [109, 114]. For instance, graded FeMnCoCrAl HEA thin films were fabricated via simultaneous codeposition from four separate magnetron sources, Fe-Mn, Co, Cr, and Al, onto a silicon substrate [114]. This technique is particularly suitable for synthesizing functional alloys, where performance is primarily determined by composition and crystal structure rather than microstructural features, which are more critical in structural applications. Combinatorial methods aid in HEA discovery but are insufficient to explore the entire range of possible compositions and microstructures. Furthermore, multicomponent gradients may lead to compositional overlaps and interactions, complicating the isolation of cause-and-effect relationships. This necessitates the use of advanced data analysis tools, often involving computational modeling or machine learning techniques.

1.4 | Computational Modeling

Various computational techniques, including first-principles calculations [115–119], molecular dynamics (MD) [120–125], and CALculation of PHAse Diagrams (CALPHAD) [107, 108, 126–128], have been employed to design HEAs.

1.4.1 | First-Principles (or Ab Initio) Calculations

First-principles or ab initio calculations utilize quantum mechanics to predict material properties without relying on experimental data or empirical inputs. These methods, often grounded in density functional theory (DFT), enable the precise modeling of electronic structures, phase stability, and mechanical properties [116, 118]. The four commonly used first-principles-based methods to model the disordered crystal structure of HEAs include the coherent potential approximation (CPA) [115, 118, 119, 129], virtual crystal approximation (VCA) [115, 116], special quasi-random structures (SQS) [118, 129–131], and small set of ordered structures (SSOS) [118, 132], as illustrated in Figure 3. The VCA is a mean-field method that simulates disordered alloys by substituting real atoms with virtual atoms whose properties are a weighted average of the constituent elements [115]. The mean-field characteristic of the VCA enhances computational efficiency by simplifying the complex disorder; however, it fails to capture local atomic variations. The VCA method has been applied to predict the elastic constants, ideal tensile strength, and shear strength of a single-phase TiVNbMo HEA [116]. Similarly, the CPA method, also based on mean-field theory, treats all atoms in an alloy as equivalent, modeling each atom as if it exists in a random environment. It employs a self-consistent, effective medium to represent the system, making it a computationally efficient method suitable for complex alloy systems [117]. However, the CPA's accuracy is limited, as it overlooks local lattice distortions and variations in individual atom positions [115, 118]. Despite this, CPA is more realistic than VCA because it retains the individual atom types in the model and accounts for the randomness in the alloy. Liu et al. [119] employed the CPA approach to calculate the elastic constants and mechanical properties of the refractory $Ti_{30}Zr_{30}Nb_{20}Mo_{20}$ HEA, and their findings showed good agreement with experimental data.

The SQS approach models the disordered structure of HEAs by utilizing relatively small supercells and optimizing a quasi-random crystal structure to closely resemble the key features of a random solid solution, such as nearest neighbor pairs and multisite correlation functions [130]. Unlike the VCA and CPA, the SQS method considers local lattice distortions, making it particularly effective for systems with significant atomic-size mismatches. However, because SQS uses small periodic supercells to simulate randomness, it may not fully capture long-range disorder. It can introduce artificial periodicity that is not present in truly random alloys [118]. Xie et al. [130] applied SQS to investigate the FCC $Co_{30}Ni_{30}Fe_{20}Cr_{20}$ HEA and found a lattice constant of 3.485 Å (within 2% of the experimental data) and a formation enthalpy of −1.17 eV $atom^{-1}$, suggesting structural stability. The SSOS method determines HEA properties using a weighted average over a small set of ordered structures (SOS), typically only a few atoms per unit cell [132]. These structures are designed using a generalized cluster description to capture the interactions in multicomponent systems, significantly reducing the model size and offering a lower computational cost compared to the SQS method. In conclusion, although the SQS and SSOS methods effectively capture lattice distortions in HEAs, they are more computationally demanding than the CPA and VCA. However, as the number of alloying elements increases, constructing small supercells that accurately represent the chemical disorder becomes increasingly challenging.

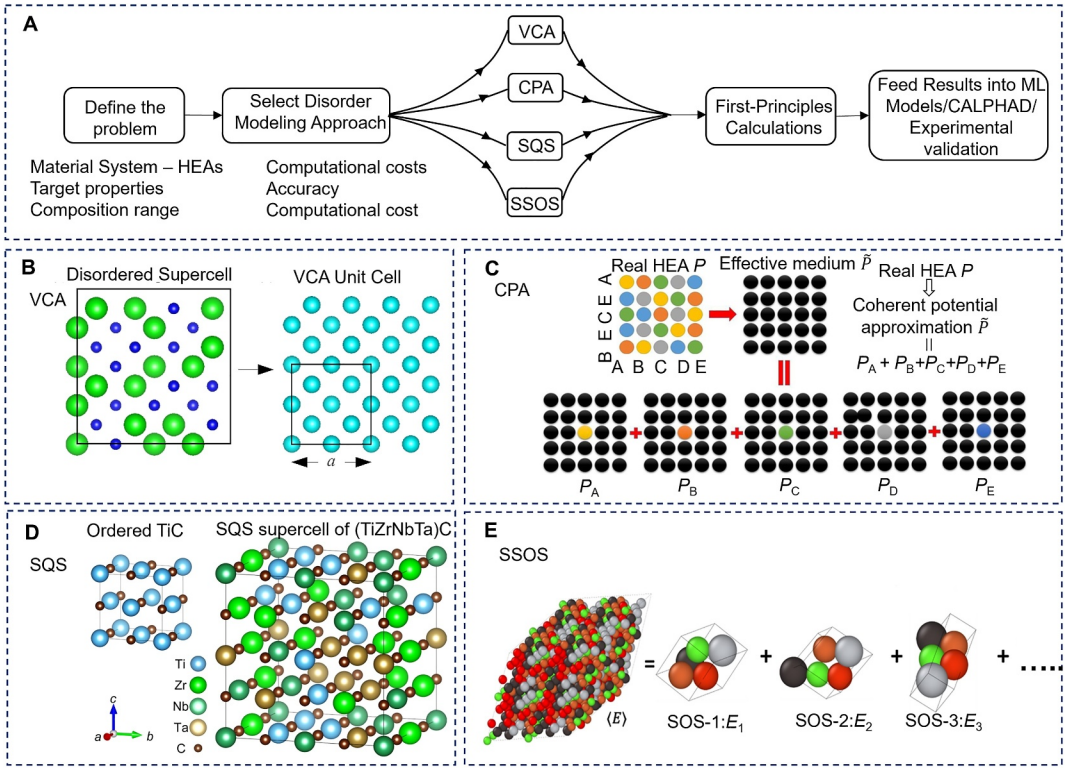

FIGURE 3 | Schematic overview of first-principles-based approaches and model systems used to describe disordered crystal structures in HEAs. (A) Simplified workflow of first-principles-based methods for modeling disordered crystal structures in HEAs. (B) Disordered supercell and VCA cell equivalent. (C) Two-dimensional schematic of the CPA for equimolar ABCDE HEAs, where P is the real alloy potential, $\tilde{P}$ the coherent potential, and $P_A - P_E$ the potentials of individual alloying elements. Reproduced with permission from Ref. [129]. Copyright 2017, the authors. (D) Rock-salt lattice of TiC and SQS supercell of (TiZrNbTa)C generated to mimic random distribution of transition-metal atoms for first-principles calculations. Reproduced with permission from Ref. [131]. Copyright 2022, Springer Nature. (E) Target HEA sample and a set of 5-atom small ordered structures (SOS). Reproduced with permission from Ref. [115]. Copyright 2023, the authors.

1.4.2 | Molecular Dynamics (MD) Simulation

Molecular dynamics (MD) simulation models materials at the atomic scale by considering atoms and molecules as interacting particles governed by classical mechanics principles. This method is particularly beneficial for investigating the mechanical properties and deformation behavior of HEAs, as it captures the microstructural evolution and uncovers the underlying deformation mechanisms at the atomic level [120–124]. Li et al. [121] employed MD to investigate the influence of strain rate and temperature on the mechanical properties and deformation behavior of nanocrystalline $Co_{25}Ni_{25}Fe_{25}Al_{17.5}Cu_{17.5}$ HEA. The MD simulation results indicated that dislocation slip dominated the deformation at low temperatures and high strain rates, whereas grain boundary sliding became the primary mechanism at higher temperatures and lower strain rates. Yang et al. [122] used MD simulations to investigate the mechanical properties of Al_xCoCrFeNi HEA, showing that the computed lattice constant, elastic constants, bulk modulus, Young's modulus, and Poisson's ratio were consistent with both experimental data and DFT results. MD simulations have also been applied to study phase transformation phenomena in CoNiCrFeMn [123] and $Al_{0.3}$CoCrFeNi HEAs [124]. Although MD simulations provide valuable atomic-level insights into the behavior of HEAs, including the ability to model complex compositions, predict mechanical properties, and examine deformation mechanisms under various conditions, they also have limitations. These include high computational costs, restricted time and length scales, and dependence on the accuracy of interatomic potentials, which can be challenging to develop for multicomponent systems such as HEAs [125].

1.4.3 | Calculation of Phase Diagram (CALPHAD)

The CALPHAD method is used to predict the phase diagrams and thermodynamic properties of materials with multiple components. It achieves this by minimizing the total Gibbs free energy of the system, utilizing inputs such as temperature, pressure, and overall composition, along with the Gibbs energy functions found in thermodynamic databases [127]. CALPHAD is widely acknowledged as a reliable and efficient method for designing alloys, as it can predict the thermodynamic properties of complex multicomponent systems by extrapolating from simpler, lower-order systems. A significant advantage of the CALPHAD method is its computational efficiency, which allows it to reduce the extensive compositional design spaces of HEAs to a few experimental trials [107, 108, 126]. By combining parametric and CALPHAD methods, Tazuddin and Biswas [107] effectively narrowed down 1287 equiatomic quinary alloys to 10 potential single-phase FCC and BCC HEAs. Of these, only two FCC and seven BCC alloys required experimental synthesis.

X-ray diffraction and scanning electron microscopy enabled the rapid identification of optimal alloy compositions.

Klaver et al. [108] employed the CALPHAD method to refine an initial design space of more than 3 million compositions in six-element alloy systems (AlCrMnNbTiV and AlCrMoNbTiV) and five-element systems (AlCrFeTiV and AlCrMnMoTi) to select a few candidates for experimental investigation. Their goal was to identify compositions that form single-phase solid solutions and exhibit good oxidation resistance at relatively low temperatures. Compositions near $Al_{25}Cr_7Mn_{25}Nb_1Ti_1V_{41}$ and $Al_{21}Cr_7Mn_{21}Nb_1Ti_9V_{41}$ met both criteria, exhibiting high-entropy phase stability at 800 K and containing high levels of Al and/or Cr, which enhance oxidation resistance. Conway et al. [126] used the CALPHAD method to screen 1.78 million compositions within the Co-Cr-Fe-Ni-Mn alloy system, ultimately identifying the $Co_{10}Cr_{12}Fe_{43}Mn_{18}Ni_{17}$ alloy. This alloy demonstrated excellent high-temperature strength and ductility, along with a 40% cost reduction compared to the equiatomic Cantor alloy. Recognizing twinning-induced plasticity and solid-solution hardening as key strengthening mechanisms in these alloys, the authors suggested integrating models for stacking fault energy, solid-solution hardening, and cost into high-throughput screening algorithms to accelerate the design of alloys with targeted mechanical properties. Although CALPHAD is a robust tool for predicting phase stability and guiding alloy design, its accuracy depends on the availability and quality of comprehensive thermodynamic databases, especially those covering wide compositional and temperature ranges. Moreover, CALPHAD focuses on equilibrium thermodynamics and does not account for kinetic factors or metastable phases. It also does not directly predict mechanical properties, and large-scale high-throughput applications can be computationally intensive. Conversely, machine learning can rapidly analyze extensive datasets to capture complex relationships among composition, microstructure, and properties. This enables faster property prediction, composition optimization, and the discovery of novel high-performance HEAs. This shift from conventional methods to ML-based methods marks a significant advancement in HEA research, offering a more efficient, data-driven framework for alloy design.

1.5 | The Rise of Machine Learning in Materials Science

1.5.1 | Core Advantages of Machine Learning in Accelerating Materials Discovery

Machine learning is a powerful computational method that enables predictive modeling by recognizing complex patterns in large datasets [133]. In alloy design, ML can reveal the underlying trends and correlations in material data, thereby enhancing the efficiency and precision of the design process. ML builds an optimal function that links inputs to outputs in a training dataset, allowing the prediction of unknown outputs from new inputs. ML algorithms are categorized into supervised, unsupervised, semi-supervised, and reinforcement learning [134, 135]. In material design, supervised learning is used to predict material properties based on known experimental data. This algorithm learns from labeled data, where both the inputs and the corresponding outputs are provided. The most commonly employed supervised learning algorithms include support vector machines (SVMs), random forests, k-nearest neighbors (kNNs), and neural networks (NNs) [133, 135, 136]. Conversely, unsupervised learning utilizes data without labeled responses, aiming to discover hidden patterns and structures and is primarily applied in clustering, dimensionality reduction, and generative modeling [135, 136]. Semi-supervised learning involves the use of a large volume of unlabeled data in conjunction with a small set of labeled data. In contrast, reinforcement learning operates without explicit input-output pairs, instead relying on feedback from actions to maximize a reward signal, guiding the model to learn optimal behaviors within an environment [135]. The ML process typically involves several key stages, as illustrated in Figure 4. Data are collected and preprocessed to ensure that they are clean, consistent, and properly formatted for analysis. The data are then split into training and testing subsets. An appropriate model is then selected and trained using the training dataset. The model's performance is evaluated on the test set using metrics such as accuracy and precision. Based on this evaluation, the model can be fine-tuned and adjusted. Ultimately, the optimized model is deployed for practical use, where it is continuously monitored and updated as needed to maintain its efficacy.

Raccuglia et al. [139] demonstrated the effectiveness of ML in accelerating materials discovery by converting large amounts of previously "failed" experimental data into a resource for material innovation. They successfully trained an ML model to predict the outcomes of crystallization reactions in inorganic-organic hybrid materials, achieving an impressive accuracy of 89% in identifying the formation of new compounds. Although the accuracy of ML techniques depends heavily on high-fidelity experimental datasets for accurate training, Meredig et al. [140] illustrated the synergy between ML and DFT, demonstrating how first-principles calculations can enhance data-driven approaches for material discovery. By utilizing a database containing thousands of DFT calculations, an ML model was trained to predict the thermodynamic stability of arbitrary compositions, resulting in a six-order-of-magnitude reduction in computational cost compared to DFT [140]. This model enabled the screening of approximately 1.6 million ternary compositions, resulting in the prediction of more than 4500 previously unknown stable materials. Conducting such an extensive analysis using first-principles calculations would be computationally infeasible and impractical to perform experimentally, underscoring the capability and scalability of ML in accelerating material discovery. When is it suitable to use ML for materials discovery? ML is particularly advantageous in scenarios where traditional methods encounter substantial constraints. As emphasized by Ramprasad et al. [141], data-driven methods are best suited for predicting properties that are either too costly or time-consuming to compute or to measure experimentally. They are also effective when dealing with complex or stochastic phenomena that do not lend themselves to direct solutions through fundamental equations or when the underlying physical laws governing a system remain unknown, thereby justifying the use of surrogate models to approximate behavior.

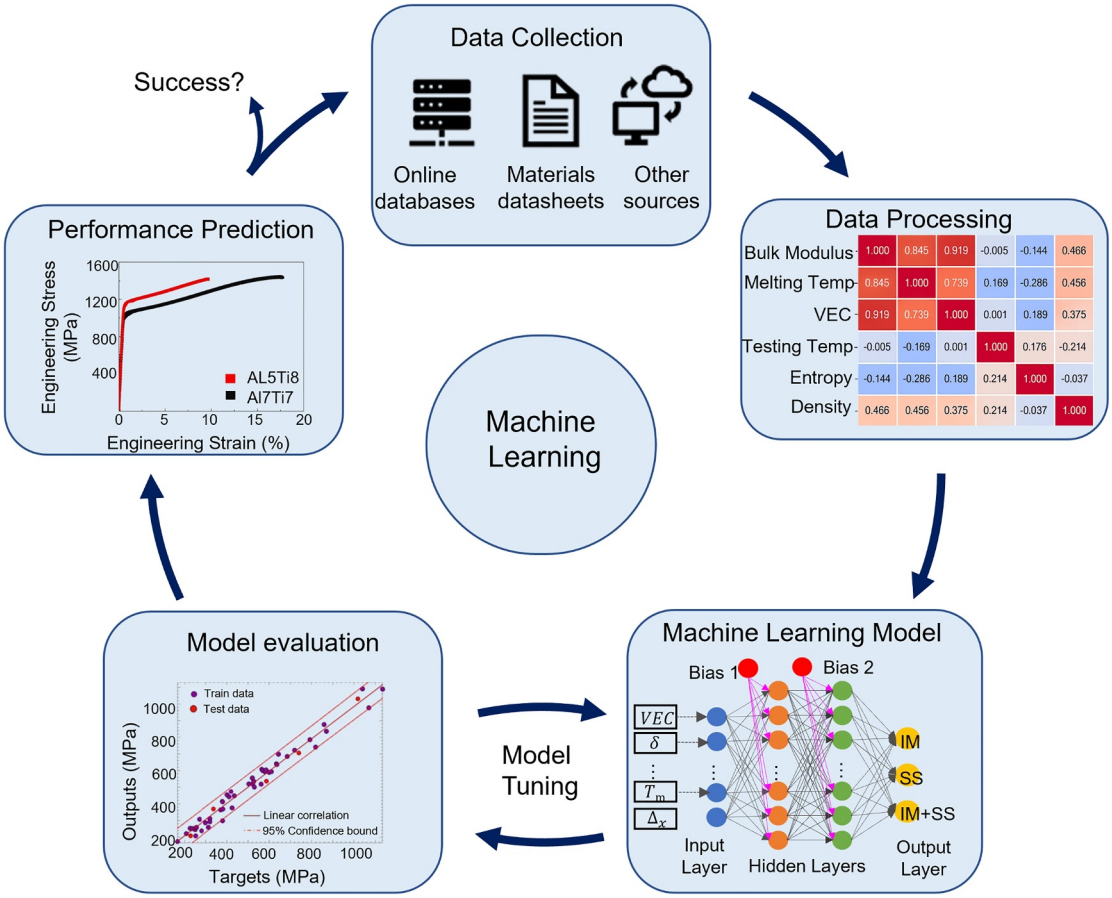

FIGURE 4 | A typical workflow for machine learning in material discovery. The process begins with data collection and processing, followed by model training and evaluation. Once validated, the trained models are used to predict material properties from composition and other material parameters, enabling accelerated material design [7, 137, 138].

1.5.2 | The Synergy Between ML and HEA Research

Although the increased number of principal elements in HEAs presents significant opportunities for alloy design, it also introduces considerable challenges in theoretical modeling and simulations. These challenges arise from the complexity involved in developing accurate empirical atomic interaction models owing to the numerous chemical interactions and the high computational cost of first-principles methods, such as DFT. This method requires large supercells to accurately represent the complex structural and chemical features of HEAs [142]. Moreover, high-throughput simulations generate extensive data characterized by high-dimensional inputs and low-dimensional outputs, which present significant challenges for traditional modeling techniques [143]. Furthermore, the conventional trial-and-error approach to material design is impractical for exploring the vast compositional space of HEAs, highlighting the need for efficient predictive models.

The strength of ML lies in its ability to capture complex, nonlinear patterns through models that can be systematically optimized via data-driven learning. In the context of HEAs, ML algorithms excel at navigating the vast, high-dimensional compositional space to identify promising alloy candidates with targeted properties, significantly minimizing dependence on traditional trial-and-error methods [144]. Additionally, ML models offer a computationally efficient alternative to first-principles methods, such as DFT, by approximating interatomic potentials with near-DFT accuracy at a fraction of the computational cost. This efficiency enables the simulation of systems with millions of atoms, which is essential for accurately modeling the microstructural complexity, defect behavior, and phase transformations that define HEAs. Furthermore, the integration of traditional methods with ML is rapidly advancing in HEA research, aiming to harness the synergy between them by leveraging their respective strengths [142–145]. Driven by advancements in computing power, algorithm development, and the increasing availability of high-quality experimental and computational data, ML has become an indispensable tool for addressing the fundamental challenges of HEA design and modeling. Common ML models used in HEA design include k-nearest neighbors (kNNs) [7, 146], support vector machines (SVMs) [5, 7, 146], Gaussian processes (GPs), random forests (RFs) [5, 138, 146], logistic regression (LR) [5], gradient boosting decision trees (GBDT) [5], and neural networks (NNs) [5, 7, 142, 143, 146–150].

1.6 | Review Objectives

This review examines the integration of ML in HEA research, with a focus on its core applications in the field. Key areas of

progress include ML-driven methods for composition design, phase prediction, performance prediction, microstructure analysis, and process parameter optimization. In addition, this review examines existing challenges and highlights recent technical breakthroughs that are expanding the scope and enhancing the reliability of ML in materials science. This study also highlights the growing synergy among experimental, computational, and data-driven approaches, which is crucial for accelerating material discovery in this rapidly evolving field.

2 | Core Applications of ML in HEA Research

2.1 | Composition Design and Phase Prediction

The properties of materials are highly dependent on their phase constitution. Different phases in HEAs, such as solid solution (SS), amorphous (AM), intermetallic (IM), or a combination of SS and IM, enable the tailoring of material properties to meet specific performance requirements. Therefore, accurate prediction of the phase that will form for a given composition is essential for guiding alloy design. Conventional computational and experimental methods for phase prediction are often slow and limited in scope, whereas ML enables rapid phase prediction by leveraging existing datasets across vast compositional spaces. Islam et al. [147] employed an NN to predict phase formation (SS, AM, or IM) based on five key input features from a dataset of 118 experimentally studied HEAs, as illustrated in Figure 5A. The input features included valence electron concentration (VEC), difference in Pauling electronegativities $\Delta\chi$, atomic size difference δ, ΔH_{mix}, and S_{mix}. The trained NN achieved an accuracy exceeding 99% for the complete dataset. However, fourfold cross-validation showed an average generalization accuracy of 83%, suggesting some overfitting. This discrepancy was attributed to the limited size of the dataset, underscoring the need for larger datasets to enhance the model's robustness. Feature importance analysis revealed the following order of influence on phase prediction: $VEC > \Delta\chi > \Delta H_{mix} > \delta > S_{mix}$, indicating that VEC is the most critical factor for determining phase formation in HEAs, as shown in Figure 5B. This study demonstrates the capability of NN to accurately predict phase formation in HEAs based on key thermodynamic and atomic descriptors, highlighting ML as a valuable tool in material design. It also highlights the importance of large, high-quality datasets to ensure reliable model generalization and prevent overfitting in data-driven materials research.

Liu et al. [142] developed an ML framework by integrating first-principles calculations with an ANN to explore the phase stability and elastic properties of the AlCoCrFeNi HEA system, encompassing both FCC and BCC phases. The ANN was trained using 0 K first-principles data, with elemental concentrations as inputs and the enthalpy of formation (ΔH_f) and elastic constants as outputs. By employing the OPTUNA optimization framework

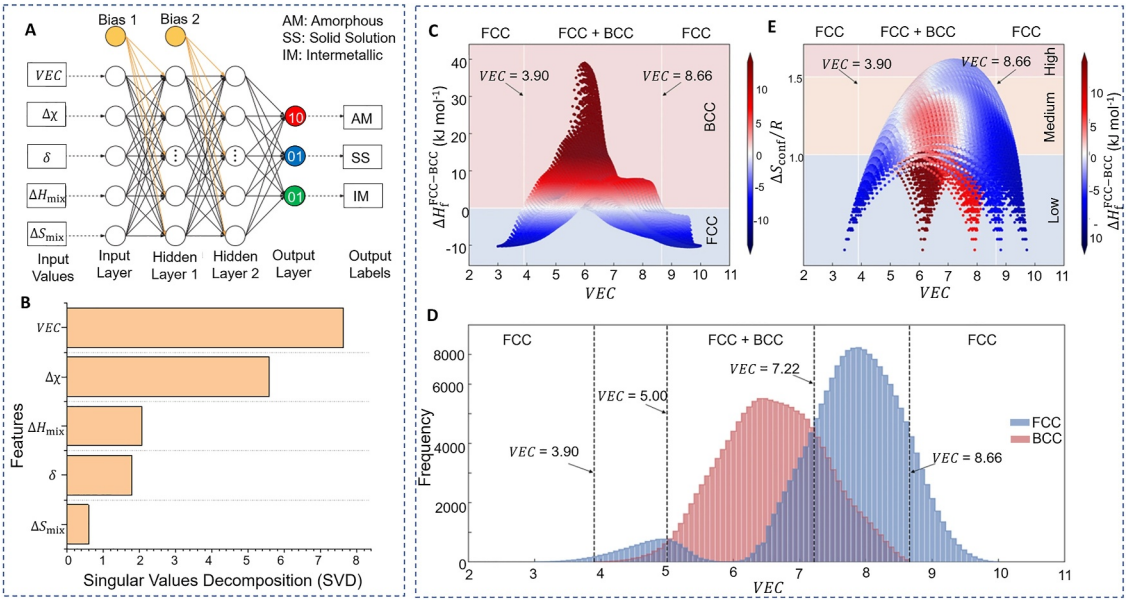

FIGURE 5 | Machine learning for phase prediction. (A) A sample NN architecture for phase prediction in HEAs. It has two hidden layers, each with five neurons (circles) for clarity. Inputs and outputs are empty squares. Phases AM, SS, and IM are encoded as (100), (010), and (001), respectively. (B) Feature importance analysis indicating that VEC is the most critical factor for determining phase formation in HEAs. Reproduced with permission from Ref. [147]. Copyright 2018, Elsevier. (C) Relationship between VEC and $\Delta H_f^{FCC-BCC}$ in the Al-Co-Cr-Fe-Ni system. The region where $\Delta H_f^{FCC-BCC} < 0$ indicates greater stability of the FCC phase, whereas $\Delta H_f^{FCC-BCC} \geq 0$ indicates greater stability of the BCC phase. (D) Relationship between statistical frequency and VEC for the occurrence of stable FCC or BCC within the analyzed VEC range. The red bars show stable BCC frequency, and the blue bars indicate stable FCC frequency. The FCC phase is more stable at VEC > 7.22 or < 5.00, peaking at < 3.90 or > 8.66. The BCC phase dominates between 5.00 and 7.22, especially near VEC ≈ 6.00. (E) Relationship between configurational entropy ($\Delta S_{conf}/R$) and VEC of FCC and BCC phases in the AlCoCrFeNi system for over 300,000 predicted data points. Only a small fraction of the Al-Co-Cr-Fe-Ni system meets the HEA criterion ($\Delta S_{conf}/R \geq 1.5$). Reproduced with permission from Ref. [142]. Copyright 2024, Springer Nature.

for hyperparameter tuning, the model established a clear relationship between VEC and $\Delta H_f^{FCC-BCC}$. As shown in Figure 5C, the region where $\Delta H_f^{FCC-BCC} < 0$ indicates greater stability of the FCC phase, whereas $\Delta H_f^{FCC-BCC} \geq 0$ indicates greater stability of the BCC phase. The model predicted that the FCC phase exhibits more stability when VEC is either >7.22 or <5.00, with the highest stability observed at VEC < 3.90 or VEC > 8.66, as shown in Figure 5D. Conversely, BCC phase stability dominates when VEC ranges from 5.00 to 7.22, especially at VEC ≈ 6.00. This is a refinement of the empirical VEC-based parameter proposed by Guo et al. [151] for predicting the phase stability of FCC and BCC solid-solution structures. The model also revealed that only a limited composition range met the HEA criterion $(\Delta S_{conf}/R \geq 1.5)$, as shown in Figure 5E. The optimal composition for the desired elastic properties was identified as $Al_8Fe_{12}Co_{30}Cr_{24}Ni_{26}$. This study underscores the synergistic potential of combining ML and first-principles methods to expedite the rational design of high-performance HEAs.

Machaka [146] developed a systematic framework, as shown in Figure 6A, for employing ML to classify the solid-solution phases of HEAs using a dataset comprising 1460 entries from 438 peer-reviewed studies, which included 36 metallurgy-specific predictor features. This framework integrates six methods of feature selection, the construction of feature ensembles, and eight ML classifiers, including RF, SVM, kNN, and NN. The performance of the classifiers was evaluated based on accuracy, kappa index, receiver operating characteristic (ROC) curves, and area under the ROC curve. RF, SVM, kNN, and NN demonstrated high accuracy rates of 97.5%, 95.8%, 94.5%, and 94.0%, respectively, along with high AUC values, as shown in Figure 6B,C, underscoring their effectiveness in phase classification. VEC was identified as the most significant descriptor, which is consistent with the findings of Islam et al. [147]. The validity of the model and the significance of ML were further demonstrated by the successful prediction of phase stabilization and transitions, as well as by resolving discrepancies between experimental and ab initio calculations for the $NiCoFeCrAl_x$ alloy system.

The vast combinatorial space of model-descriptor combinations poses a significant challenge in selecting optimal ML models and descriptors for predicting phase formation in HEAs. To address this, Zhang et al. [152] developed a framework based on

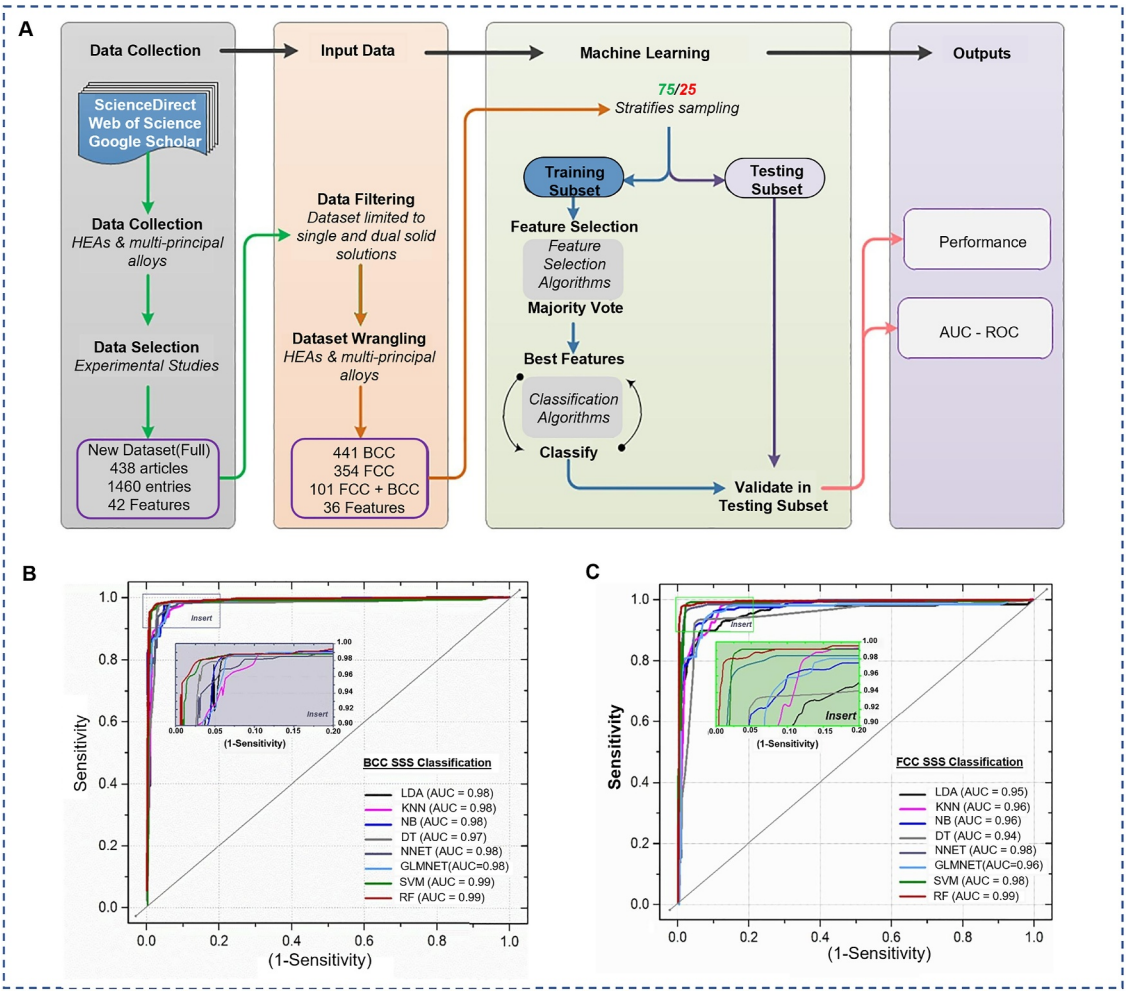

FIGURE 6 | Machine learning workflow and validation results for multiclass classification of solid-solution phases. (A) The ML framework consists of initial feature selection using all 36 features; application of Boruta, LVQ, RF-RFE, and SVM-RFE for feature reduction; ranking of features by importance via majority vote; creation of seven top-ranked feature ensembles; and evaluation of classifier performance using accuracy, kappa index, and AUC. (B) ROC curves for validating the classification of BCC single-phase solid solution and (C) FCC single-phase solid solution. Both show higher performance for RF, SVM, kNN, and NN models. Reproduced with permission from Ref. [146]. Copyright 2021, Elsevier.

a genetic algorithm (GA) to optimize both model selection and descriptor subsets, as shown in Figure 7A. The study constructed a descriptor space comprising 70 features derived from elemental, thermodynamic, structural, and DFT-based parameters and assessed nine ML classifiers, as listed in Figure 7B. GA was employed to systematically identify the optimal combination of descriptors and classifiers, significantly boosting predictive performance and achieving classification accuracies of 88.7% (Figure 7B) for distinguishing solid-solution (SS) from non-solid-solution (NSS) phases and 91.3% (Figure 7C) for differentiating FCC, BCC, and dual-phase (DP) HEAs. Huang et al. [7] employed three ML algorithms—kNN, SVM, and ANN—to classify HEA phases using an experimental dataset of 401 samples derived from the work of Miracle and Senkov [10]. The study applied five key features—VEC, δ, $\Delta\chi$, ΔS_{mix}, and ΔH_{mix}—for the theoretical correlation with the phase stability. Among the models, the multilayer feedforward neural network (MLFFNN), illustrated in Figure 8A, showed the highest average testing accuracy of 74.3% for three-phase classification and up to 94.3% for binary classifications, surpassing kNN and SVM. Figure 8B–D illustrates how the average testing accuracy changes depending on the number of neurons used in the three hidden layers of the neural network, labeled n_1, n_2, and n_3. This study further highlights the superior ability of ANN to handle the complex and nonlinear nature of HEA phase prediction, underscoring the importance of carefully optimizing the network architecture.

A significant challenge in predicting HEA phases is the scarcity of high-quality experimental data, which often leads to uneven data distributions, overfitting, and limited model generalization. To address the limitations associated with small datasets, Wu et al. [5] utilized a generative adversarial network (GAN) to augment an initial dataset of 544 HEA configurations, as illustrated in Figure 8E. The augmented data were used to train and optimize ML models, such as SVM, ANN, RF, gradient boosting decision tree (GBDT), and logistic regression (LR), via hyperparameter tuning with the Optuna framework. SVM, ANN, and RF models were used to predict the SS, IM, and AM phases, whereas RF, GBDT, and LR were applied to classify FCC and BCC structures within the solid-solution phases. The augmented dataset significantly improved model performance in multiphase classification:

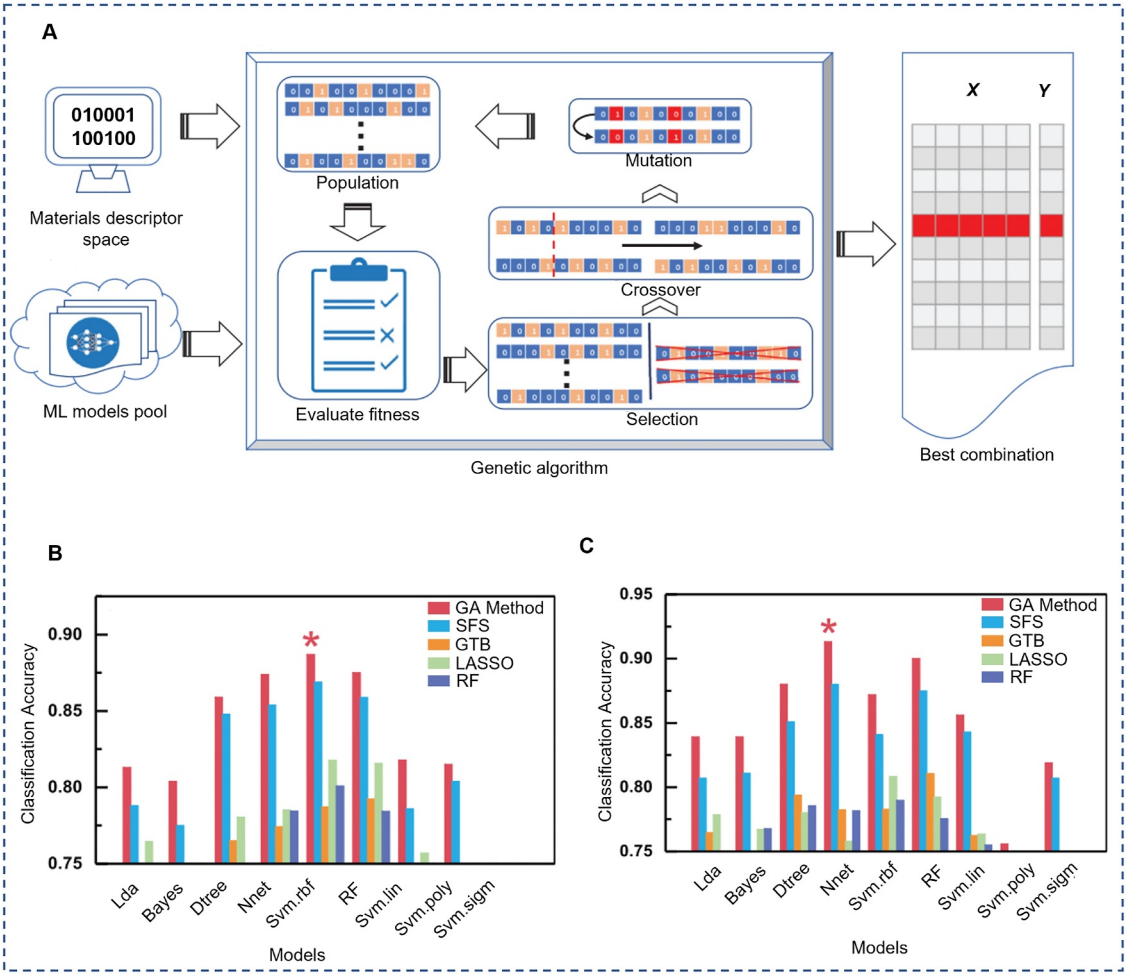

FIGURE 7 | Genetic algorithm (GA)–driven ML framework for optimizing descriptor subsets and model selection in solid-solution phase classification. (A) GA loop taking material descriptor space and ML model pool as input, iteratively optimizing a fitness function until a stopping criterion is reached, yielding the optimal model–descriptor combination. (B) Comparison of nine ML models using descriptor subsets selected by least absolute shrinkage and selection operator (LASSO), RF, gradient tree boosting (GTB), sequential feature selection (SFS), and GA. Solid-solution versus non-solid-solution classification shows SVM.rbf with GA descriptors as the best model. (C) FCC, BCC, and dual-phase classification shows NN with GA descriptors as the best model. Reproduced with permission from Ref. [152]. Copyright 2020, Elsevier.

SVM achieved 94.77% accuracy, ANN 94.3%, and RF 93.8% (Figure 8F). For the FCC/BCC classification, RF achieved the highest accuracy at 98%, followed by GBDT at 92% and LR at 85%. This approach highlights the growing trend in alloy design, where generative models are employed not only for data augmentation but also for material discovery and design. For instance, Li et al. [153] developed cardiGAN, a GAN-based framework capable of generating novel multiprincipal element alloy (MPEA) compositions with targeted phase characteristics. One of the predicted compositions, $Al_5Co_8Cu_{35}Fe_{19}Ni_{23}V_{11}$, was experimentally validated and found to form a stable FCC phase. These studies illustrate that data-driven ML techniques can effectively overcome the limitations of small experimental datasets using techniques such as data augmentation, thereby enhancing model performance and generalizability. They highlight the power of generative models to explore vast compositional spaces and accelerate the discovery of high-potential HEAs and related alloy systems. Phase prediction plays a crucial role in alloy production, as it aids in the selection of compositions that are most likely to form desired phases, which, in turn, affect the material's properties. By accurately predicting phase formation, alloy designers can narrow down potential candidates, thereby minimizing the necessity for extensive trial-and-error experimentation in the laboratory. Additionally, phase prediction helps optimize manufacturing processes by identifying alloys that are more likely to remain stable under varying processing conditions, such as different temperatures and pressures.

2.2 | Performance Prediction and Optimization

ML has also been employed in the study of complex composition–property relationships in HEAs, leading to the design of alloys with customized mechanical and functional properties. The development of HEAs with high yield strengths at elevated temperatures remains a significant challenge due to the inherent complexity of the alloys and the associated costs and difficulties in conducting high-temperature experiments on them. To address this, Bhandari et al. [138] developed an ML approach using an RF regression model, shown in Figure 9A, to predict the yield strengths of HEAs at various temperatures. Using a dataset of 238 samples, which included compositional, physical, and thermodynamic features, such as density, entropy of mixing, and bulk modulus, the model was trained to predict the yield strength across a range of temperatures. After removing multicollinearity through statistical analysis, the optimized feature set was used to construct the RF model, achieving a prediction accuracy of 93%–97% (Figure 9B). The model accurately predicted the yield strengths of MoNbTaTiW and HfMoNbTaTiZr HEAs at 800°C and 1200°C, with the predicted values closely matching the experimental results. For instance, MoNbTaTiW had predicted yield strengths of 709 and 572 MPa at 800°C and 1200°C, respectively, compared with the experimental values of 674 and 585 MPa. The model was also used to predict the performance at 1500°C, demonstrating its potential for high-temperature applications where experimental

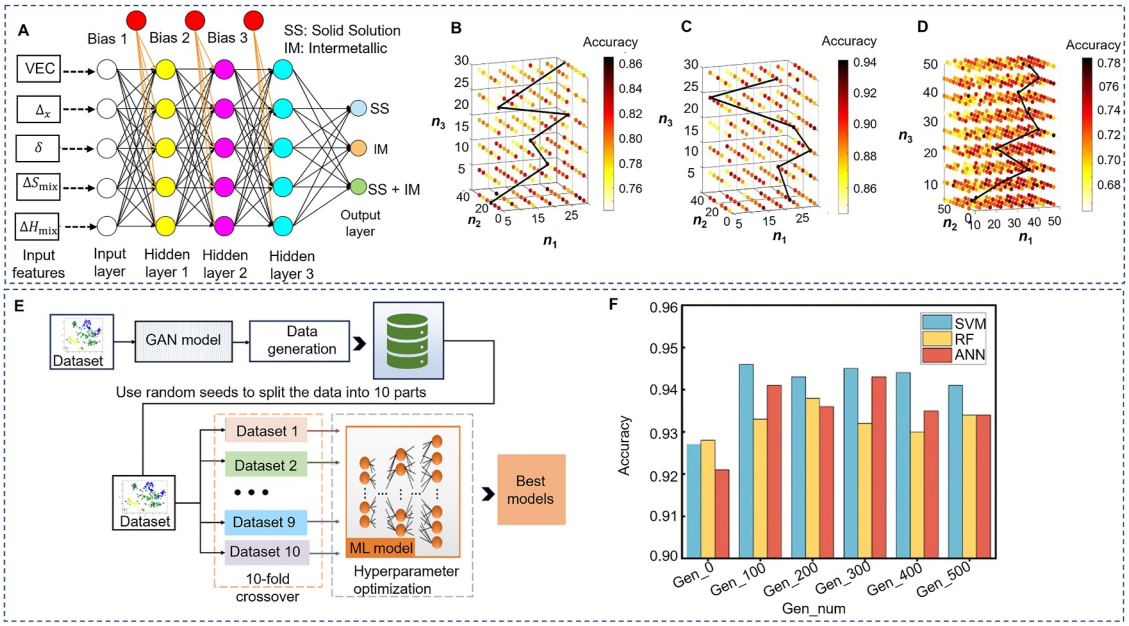

FIGURE 8 | Neural network architecture, classification performance, and GAN-based data augmentation for improved solid-solution phase prediction. (A) A multilayer feedforward neural network (MLFFNN) with five inputs, three hidden layers, an output layer, and three bias nodes for phase classification. (B) Scatter plots corresponding to the binary classification task using the MLFFNN for SS and IM; (C) SS + IM and IM; (D) SS and SS + IM. The darker the color in the scatter plot, the higher the accuracy. The solid black lines connect the data points corresponding to the highest testing accuracy for a fixed n_3, as n_1 and n_2 vary from 5 to 30 in Panels (B) and (C) and from 10 to 50 in Panel (D). The viewpoint of these plots is parallel to the $n_1 - n_2$ plane. Reproduced with permission from Ref. [7]. Copyright 2019, Elsevier. (E) Integration of ML and generative adversarial network (GAN) models for data augmentation and model optimization. GAN-based augmentation generated five datasets (100–500 samples), each merged with the original data. The augmented datasets underwent tenfold cross-validation and hyperparameter tuning to optimize model performance. (F) Prediction accuracy of the model before and after data augmentation. Labels such as "Gen_0" to "Gen_500" indicate datasets consisting of the original data augmented with 0–500 GAN-generated samples. The plot shows that augmenting the dataset leads to noticeable improvements in accuracy across all three models. Reproduced with permission from Ref. [5]. Copyright 2024, Royal Society of Chemistry.

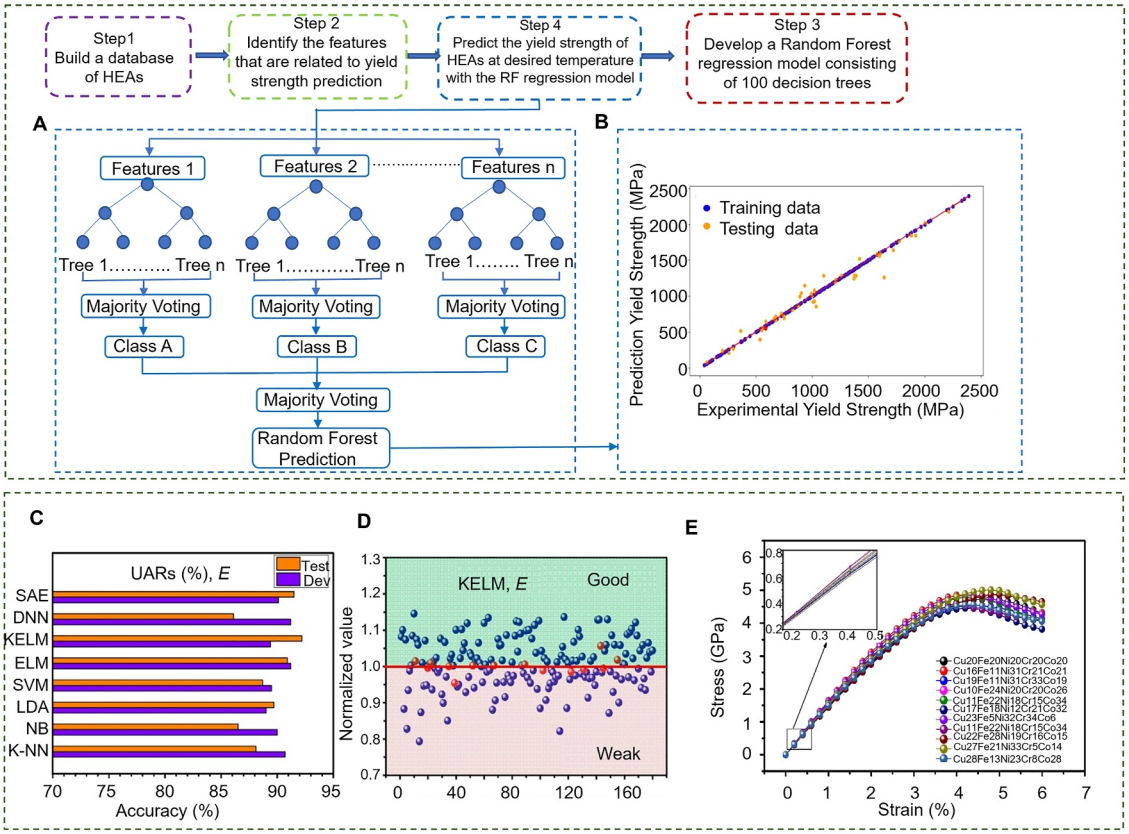

FIGURE 9 | Application of supervised learning models for predicting and evaluating mechanical properties of HEAs, including yield strength and Young's modulus. (A) A general flowchart of the random forest regressor model showing multiple decision trees with majority voting. (B) Yield strength predictions at 800°C using the random forest regressor for MoNbTaTiW. Reproduced with permission from Ref. [138]. Copyright 2021, Elsevier. (C) Performance comparison of eight ML models for predicting the Young's modulus of CuFeNiCrCo HEAs. Panel (D) shows the KELM model prediction results for the test set for Young's modulus. In this panel, the red line represents the benchmark value from the equiatomic sample; points above the line are classified as "good," whereas points below are classified as "weak." (E) Stress-strain curves of polycrystalline HEA samples with varying compositions under uniaxial tension, highlighting the effect of elemental composition on mechanical performance. Reproduced with permission from Ref. [154]. Copyright 2021, the authors.

data are limited. This study highlights the potential of ML methods, particularly RF models, to expedite HEA design by providing accurate and cost-effective predictions of key mechanical properties in scenarios where conventional experimental methods are challenging to implement or impractical.

Zhang et al. [154] successfully leveraged the synergy between MD simulations and ML to predict the mechanical properties of nonequiatomic CuFeNiCrCo HEAs. The researchers built an extensive database from the tensile test results of 900 single-crystal HEA samples generated through MD simulations, capturing the complex relationship between the elemental composition and mechanical behavior. They examined eight ML models: Naive Bayes (NB), k-NN, linear discriminant analysis (LDA), SVM, extreme learning machine (ELM), kernel-based extreme learning machine (KELM), deep neural network (DNN), and stacked autoencoders (SAE). Among these, the KELM model emerged as the most effective, achieving approximately 90% accuracy for yield stress prediction and an unweighted average recall (UAR) of 92.2% for Young's modulus (Figure 9C). The robustness of the model was further validated by the successful prediction of the mechanical performance of large-sized HEA polycrystals, demonstrating strong generalization beyond single-crystal data (Figure 9E). This study highlights the powerful potential of integrating computational simulations with ML techniques to accelerate the prediction and optimization of mechanical properties, thereby addressing the challenge of data scarcity.

The discovery of HEAs with optimal mechanical properties remains challenging owing to the vast compositional space and the inefficiencies of traditional trial-and-error methods. Recent initiatives have increasingly focused on leveraging ML and active learning frameworks to expedite the discovery of HEAs with enhanced hardness, as illustrated in the studies by Wen et al. [144] and Zhao et al. [155]. Wen et al. [144] developed an ML-assisted framework for designing HEAs with enhanced hardness within the Al-Co-Cr-Cu-Fe-Ni system. The overall approach, which integrates ML with an iterative experimental design (Figure 10A), employs two parallel strategies: one based solely on compositions and the other incorporating physical descriptors to systematically guide the discovery of alloys. A dataset of 155 experimentally measured HEAs was assembled from the literature and in-house experiments to train and validate the models, representing only a small fraction of the nearly 1.9 million possible compositions generated by discretizing the

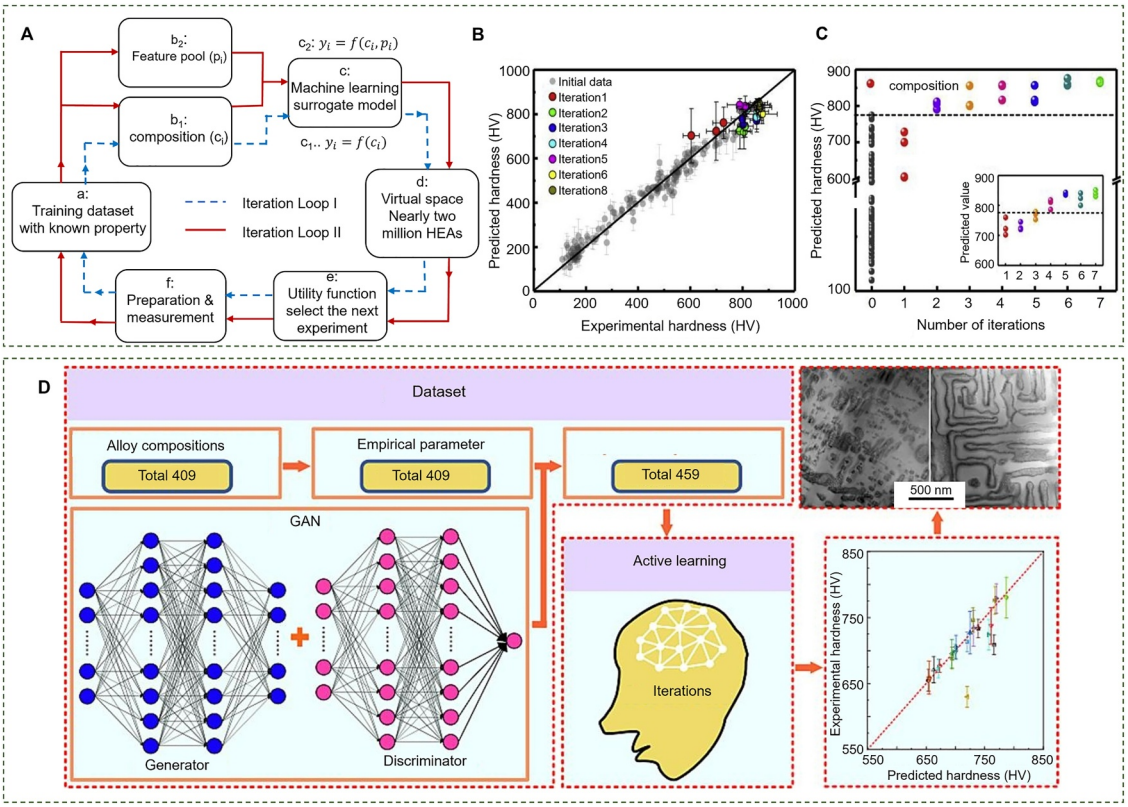

FIGURE 10 | Leveraging ML and active learning frameworks for accelerated HEA design and optimization. (A) Iterative ML and design of experiments (DOE) frameworks for the accelerated design of HEAs with enhanced hardness. Iteration Loop I uses compositions alone to train an ML surrogate model, predict hardness, and guide experimental selection via an expected improvement (EI) utility function. Iteration Loop II improves the model by incorporating physical descriptors related to elemental properties, thereby enhancing the search efficiency and accuracy of the model. The experimental feedback after each iteration continuously refines the model to discover alloys with superior hardness. (B) Performance of the iterative ML-guided alloy design strategy (Iteration Loop II) indicating predicted versus experimentally measured hardness of alloys synthesized during successive iterations, showing strong agreement and model robustness. (C) Evolution of the measured hardness across iterations, with newly discovered alloys consistently surpassing the maximum hardness of the original training dataset. The methodology demonstrated rapid convergence toward superior alloys within only seven experimental cycles. Reproduced with permission from Ref. [144]. Copyright 2019, Elsevier. (D) A machine learning framework incorporating GAN to augment the data and active learning to screen the Al-Co-Cr-Cu-Fe-Ni system. The GAN architecture includes a generator and discriminator. The generator takes random noise matching the input data's dimensions and learns to produce synthetic data that mimic the original distribution. Reproduced with permission from Ref. [155]. Copyright 2024, Elsevier.

compositional space at 1 at% intervals. Various ML models, including linear regression, support vector regression (SVR), decision trees, k-NN, and NN, were evaluated. Among them, SVR with a radial basis function kernel (SVR.r) was chosen for its superior performance, as determined by tenfold cross-validation and the bootstrap method. The methodology integrated ML predictions with an expected improvement (EI) utility function to iteratively guide the selection of alloys. The experimental results from each cycle were incorporated back into the training set to progressively refine the model, ultimately leading to the discovery of Al-rich and Cu-lean compositions exhibiting a hardness up to 14% greater than that of the best alloy in the initial dataset.

Building upon these advances, Zhao et al. [155] further expanded the methodology by incorporating a larger initial dataset (409 alloys), using generative adversarial networks (GANs) to augment the data, and employing active learning with extreme gradient boosting (XGBoost) as the master model (Figure 10D). This framework evaluated nearly 4 million potential compositions within the Al-Co-Cr-Cu-Fe-Ni system, discovering Al-rich HEAs ($Al_{46}Co_{21}Cr_{16}Cu_5Fe_0Ni_{12}$ and $Al_{40}Co_{16}Cr_{33}Fe_5Ni_6$) that exhibited ultrahigh microhardness (> 740 HV) and surprisingly low densities (< 5.9 g cm^{-3}). Microstructural analysis revealed that in both studies, the increase in hardness was primarily attributed to phase transformations that favored the hard BCC and B2 structures. Zhao et al. [155] specifically attributed this strengthening to the precipitation of disordered Cr-rich BCC nanoparticles within an ordered AlCo-rich B2 matrix. As shown in Figure 10B,D, the strong correlation between the predicted and experimental hardness values in both studies highlights the effectiveness of integrating ML models with active learning strategies for efficient HEA design. These advancements in ML-driven HEA design not only demonstrate the rapid optimization of mechanical properties, such as hardness and strength, but also suggest promising avenues for extending similar frameworks to other critical properties, including corrosion resistance, thermal stability, and wear resistance of HEAs.

In addition to elemental, thermodynamic, physical, and compositional features, fabrication methods are increasingly being incorporated as input parameters in property-prediction models. This integration is essential because different processing techniques can produce significant variations in properties, even among HEAs with the same composition [148, 149]. Zhu et al. [148] developed a DNN model that specifically encodes fabrication methods, such as as-cast and laser additive manufactured (LAM), as input features via one-hot encoding, as shown in Figure 11. Using a curated dataset of 324 HEA samples (209 as-cast and 115 LAM), this model combined elemental, thermodynamic, physical, and manufacturing data to predict the Vickers hardness. To compensate for the relatively small dataset, a conditional generative adversarial network (CGAN) was employed to generate an additional 67 synthetic samples, enhancing data diversity. The improved model achieved a mean absolute error (MAE) of 44.6 and an R^2 of 0.85, surpassing the models that excluded the processing features (MAE = 61.4, $R^2 = 0.71$). These findings underscore the significance of processing history in ML models for property prediction, demonstrating that omitting fabrication features can result in systematic prediction errors. Although data augmentation with CGAN offered modest improvements owing to the limited initial dataset size, the approach established a scalable framework for future work, where larger and more balanced datasets could further enhance prediction accuracy. Bakr et al. [149] similarly emphasized the significance of the fabrication route, incorporating manufacturing route (casting or powder metallurgy) information into hardness prediction models and achieving a high regression value of 0.88 using a dataset of 427 HEA samples.

Modeling the strengthening mechanisms in ML remains a challenge, particularly because of the difficulty in obtaining accurate model parameters, such as the volume fraction and antiphase boundary energy, for complex alloys [137, 156]. To overcome these limitations, Li et al. [137] proposed a method that integrates ML with precipitation-strengthening theory to guide the design of high-strength high-entropy/medium-entropy alloys. As illustrated in Figure 12A, the authors developed a framework that combines physical strengthening models with data-driven predictions using the AutoGluon-Tabular ML platform, trained on a dataset of 21 $L1_2$-strengthened AlTiCoCrFeNi alloy specimens. The strong correlation between the predicted and experimental values for the key precipitation parameters further validated the reliability of the ML approach. This approach enabled the high-throughput screening of nearly 230,000 alloy compositions, leading to the experimental synthesis of the $Al_5Ti_8Co_{40}Fe_7Ni_{40}$ alloy, which achieved an impressive yield strength of 1.15 GPa, approximately 10% higher than that of the best previously reported $L1_2$-strengthened AlTiCoCrFeNi HEAs (Figure 12B). Li et al. [156] also effectively employed an ML regression model to predict the volume fraction of $L1_2$ precipitate phases, as well as the hardness, yield strength, and plasticity of Fe-Co-Ni-based HEAs, achieving an accuracy of 92%. Their approach facilitated the design and optimization of four Fe-Co-Ni-based HEAs with optimized

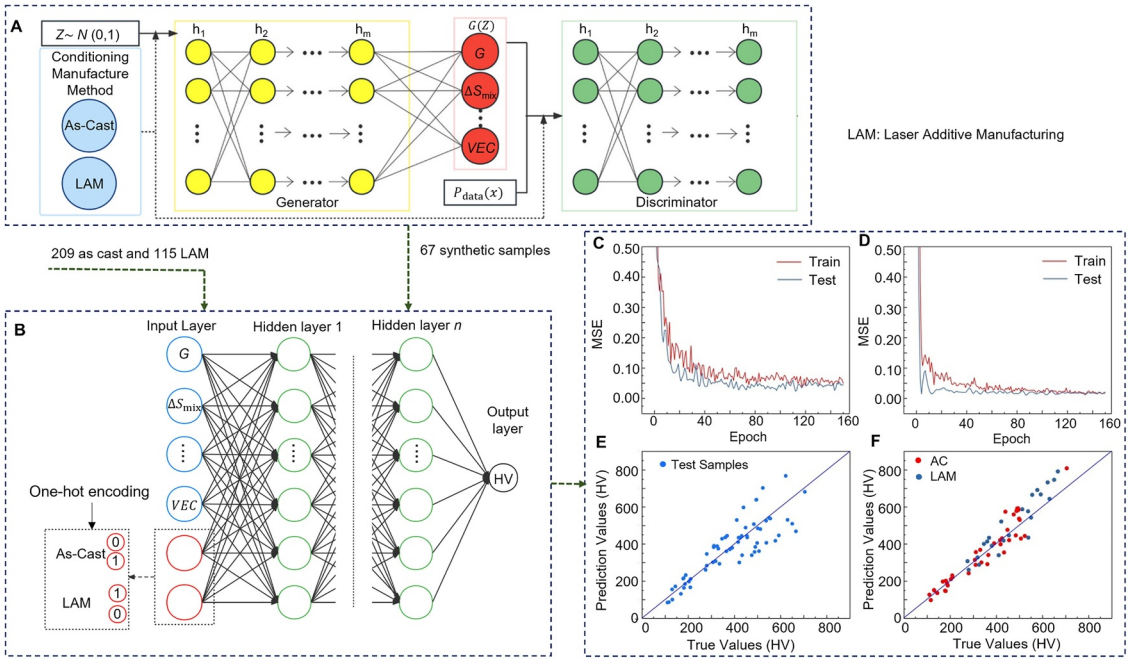

FIGURE 11 | Schematic of the DNN model integrated with CGAN model that incorporates fabrication methods as input features. (A) Conditional GAN for adversarial training that consists of mutually independent data generators and data discriminators. The generator transforms Gaussian noise into synthetic data, whereas the discriminator learns to distinguish real from generated data; after extensive adversarial training, both data types become indistinguishable, achieving effective data augmentation. (B) DNN model for hardness prediction incorporating fabrication methods, as-cast and laser additive manufactured (LAM), as one-hot encoded input features. The discrete fabrication types are encoded as "01" for as-cast and "10" for LAM, then combined with other input parameters. Panels (C, D) show the training and validation loss curves for the models without and with fabrication routes included as input features, respectively. Panels (E, F) show the prediction results for the test set, illustrating the improved accuracy and reduced error when fabrication methods (as-cast vs. laser additive manufactured) are encoded via one-hot encoding. Reproduced with permission from Ref. [148]. Copyright 2023, the authors.

microstructure and performances, as shown in Figure 12C,D. These studies demonstrate that embedding physical strengthening models into ML frameworks can significantly enhance the predictive accuracy and efficiency of alloy design, offering a scalable method for developing next-generation high-performance structural materials.

Corrosion has wide-ranging societal and economic impacts, often resulting in catastrophic damage in structural components. HEAs have emerged as a promising class of corrosion-resistant materials due to their ability to form homogeneous single phases and incorporate elements with strong passivation tendencies. However, the extensive range of possible compositions and configurational space makes discovery through trial-and-error or brute-force computation impractical. ML offers a pathway to overcome these challenges by facilitating high-throughput composition–property mapping and targeted materials selection. In a recent study, Zeng et al. [157] developed a physics-informed ML framework, as shown in Figure 13A, to identify corrosion-resistant HEAs, specifically focusing on AlCrFeCoNi systems. The approach integrated a random forest classifier, trained on an experimental dataset of 1807 entries, to predict the formability of single phases, with ML interatomic potentials trained on 1569 first-principles structures to compute surface energies and Pilling–Bedworth ratios (PBRs) for Cr oxides. This methodology enabled the mapping of these three corrosion-relevant metrics across a broad spectrum of Al and Cr compositions, showing that low Al (~< 10 at%) and ~18 at% Cr compositions are likely to produce single-phase alloys with low surface energies and appropriate PBRs, aligning with experimentally observed high corrosion resistance. The corrosion-property maps clearly identify these optimal regions, providing a data-driven basis for selecting compositions (Figure 13B–D). By directly connecting composition to passivation behavior, film compactness, and surface stability, this approach demonstrates the powerful synergy between ML and HEA design, providing not only a quicker path to corrosion-resistant alloys but also deeper mechanistic insight to guide future alloy development.

2.3 | Microstructure Analysis

Although predicting mechanical properties offers important insights into the performance of HEAs, a thorough understanding necessitates connecting these properties to the underlying microstructure. Features such as phase distribution, grain boundaries, and defect density not only determine strength, toughness, ductility, and corrosion resistance but also act as key inputs and validation points for ML models. Analyzing these microstructural parameters enables researchers to interpret observed property trends, enhance predictive models, and design alloys with optimized performance. Moreover, microstructure examination reveals how materials respond under specific conditions, such as stress, temperature, and corrosive environments, thereby aiding in predictive mechanical behavior and potential service failures. ML is increasingly being applied to microstructure analysis to automate, accelerate, and enhance the interpretation of complex material structures at the microscopic scale [158–160]. Important applications include image classification [150], microstructural segmentation [159], grain size and shape quantification, feature extraction for structure–property

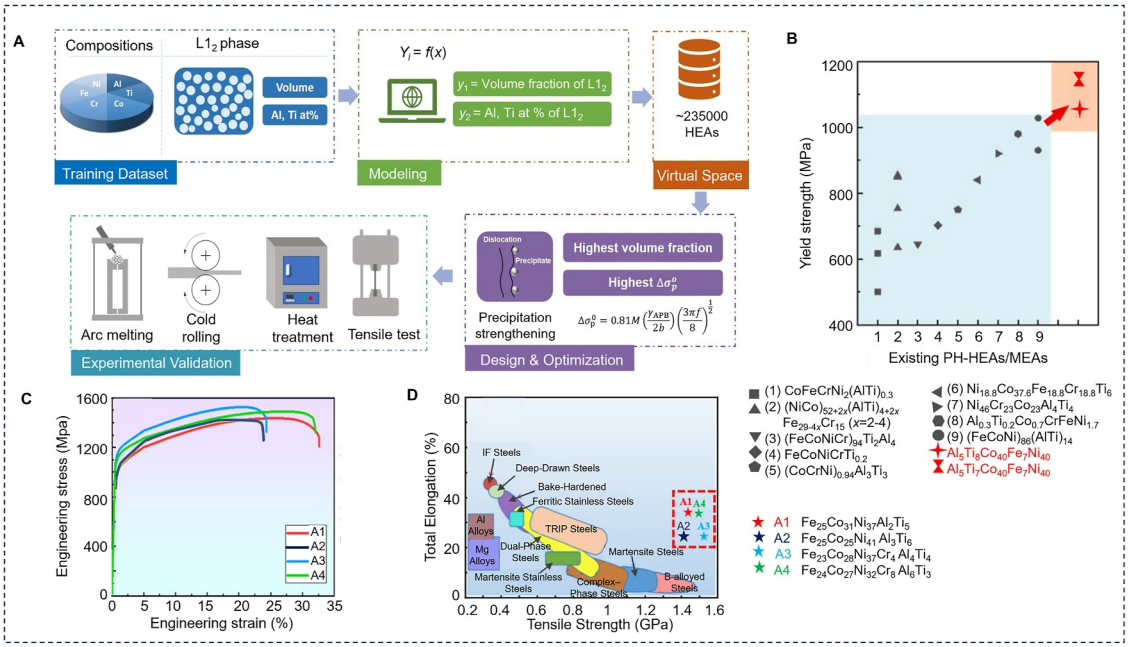

FIGURE 12 | Synergistic integration of physical strengthening models and ML enables accelerated discovery and optimization of high-strength HEAs. (A) Framework combining precipitation-strengthening theory, considering volume fraction and antiphase boundary energy of $L1_2$ nanoprecipitates, with AutoGluon-Tabular ML for alloy design. (B) Comparison of the yield strengths of the designed alloys with those of existing $L1_2$-strengthened AlTiCoCrFeNi HEAs, showing a 10% improvement with Al_5Ti_8. Reproduced with permission from Ref. [137]. Copyright 2023, Elsevier. (C) Room-temperature tensile performance of $L1_2$-strengthened Fe-Co-Ni-based HEAs discovered through ML regression across a vast compositional space and (D) the discovered alloys show excellent strength and plasticity compared with various conventional alloys. Reproduced with permission from Ref. [156]. Copyright 2024, Springer Nature.

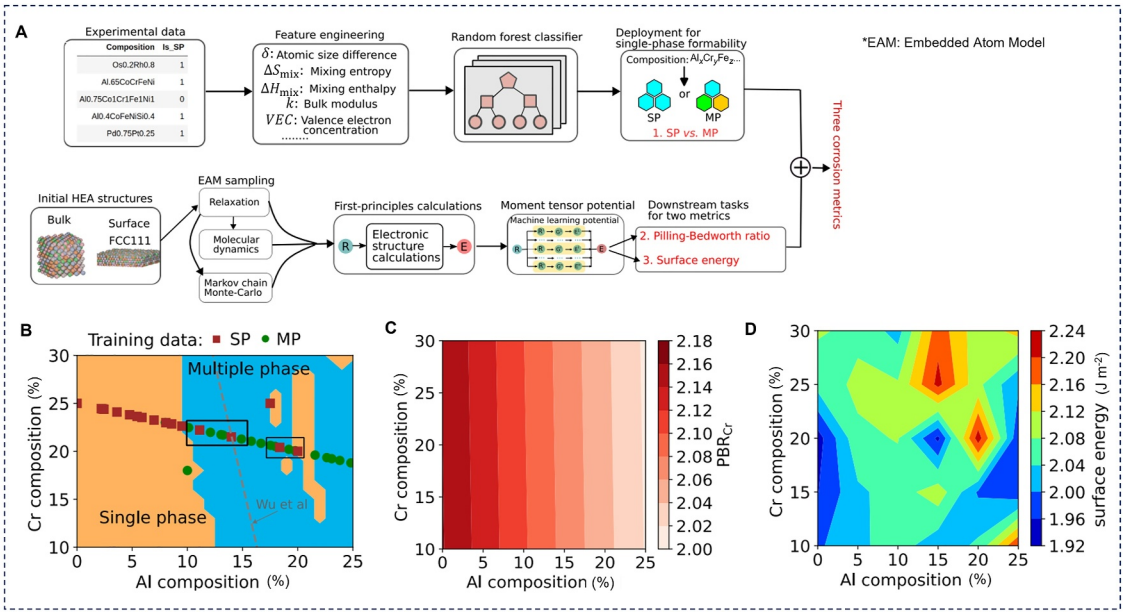

FIGURE 13 | Physics-informed ML enables accelerated discovery of corrosion-resistant high-entropy alloys by linking composition to key corrosion metrics. (A) Overview of the physics-informed ML framework used to predict corrosion resistance in AlCrFeCoNi HEAs. Composition maps of AlCrFeCoNi high-entropy alloys showing (B) single-phase formability predicted by a random forest model, (C) Pilling–Bedworth ratios for Cr oxidation, and (D) FCC (111) surface energies as a function of Al and Cr contents. Data points in Panel (B) indicate experimental training data, with red squares for single phase and green circles for multiphase alloys. The maps highlight compositional regions with low Al and ~18 at% Cr that combine desirable corrosion-resistance metrics. Reproduced with permission from Ref. [157]. Copyright 2024, Elsevier.

relationships, defect detection, and the generation of synthetic microstructures. These capabilities are particularly valuable for processing large datasets generated by advanced characterization techniques, such as X-ray diffraction (XRD), transmission electron microscopy (TEM), scanning electron microscopy (SEM), and atom probe tomography (APT). By minimizing reliance on manual interpretation, ML models not only enhance analytical throughput and reproducibility but also uncover subtle patterns that may elude traditional analysis techniques.

Biswas et al. [159] presented an innovative approach for segmenting microstructural images of steel using an ensemble of attention-guided U-Net models applied to different color-transformed images. This technique notably enhances the accuracy and robustness of segmentation in metallographic images, thereby improving the understanding of material properties and behavior. DeCost et al. [161] also employed computer vision and ML techniques, specifically bag of visual words (BoW), vector of locally aggregated descriptors (VLAD) encoding, and CNNs, to analyze and classify the complex microstructures of ultrahigh carbon steel (UHCS) from SEM images, achieving high accuracy in identifying primary microconstituents and annealing conditions. Kaufmann et al. [162] utilized two popular deep neural network architectures, ResNet-50 and Xception, to autonomously classify crystal structures from EBSD patterns, achieving overall accuracies exceeding 90% with both models. To address the issue of small data sizes, data augmentation techniques have been employed in conjunction with ML to generate synthetic data for microstructural images [163].

Despite its potential, the application of ML for the microstructural analysis of HEAs is still in its infancy. Mishra and Rahul [150] conducted a comparative study of various deep learning architectures for microstructure classification. The authors employed convolutional neural network (CNN) models, such as ResNet, DenseNet, Inception, and MobileNet, as well as ML models, including support vector classifier (SVC), tree-based models, and multilayer perceptron (MLP)-based models. These models were used to classify six distinct microstructure types: columnar, dendritic, fully eutectic, eutectic + dendritic, grain, and precipitation strengthening. The dataset comprised 500 images of nonferrous alloys, such as HEAs, superalloys, Al alloys, and Cu alloys, primarily sourced from laboratory SEM studies and the literature. By reducing the depth and width of the networks, they developed models with fewer parameters than the baseline model. The DenseNet-based model outperformed others, as shown in Figure 14B, with training, validation, and testing accuracies of 97.45%, 96.26%, and 94.89%, respectively. Figure 14A illustrates the architecture of the DenseNet-based model, which comprises 421,674 parameters (10,930 of which are nontrainable). The model consists of an input layer, convolutional layers, four dense blocks, three transition blocks, and a fully connected layer. The confusion matrix in Figure 14C illustrates the predictive performance on the test dataset, showing over 95% accuracy for all classes except the eutectic + dendritic category, which achieved slightly lower accuracy. This model was used to classify the microstructures of HEAs, $FeCoNiCrTa_{0.37}$ and $FeCoNiCrTa_{0.4}$, and the results showed good agreement. Thus, this study highlights the potential of the CNN architecture, particularly the DenseNet model, in accelerating the identification of complex HEA microstructures by effectively classifying microstructures with limited data.

Ragone et al. [164] developed a deep learning framework utilizing a fully convolutional neural network (FCN) to map the

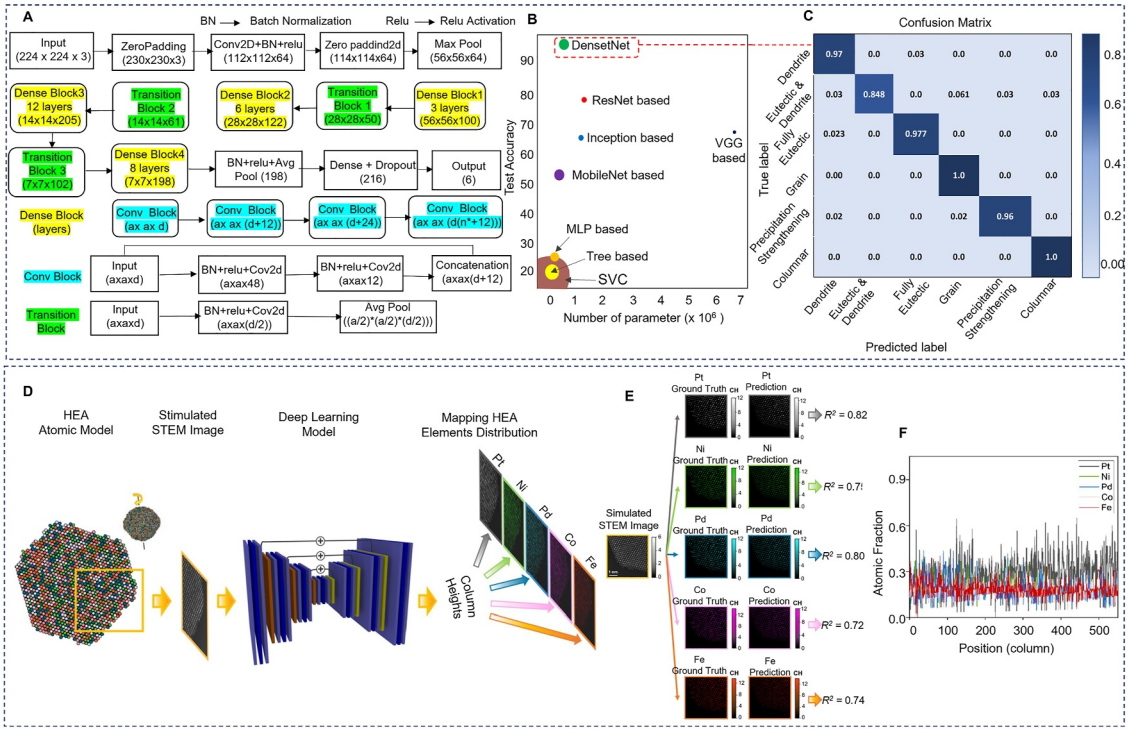

FIGURE 14 | Deep learning frameworks for microstructure classification and atomic-scale element distribution prediction in HEAs. (A) DenseNet-based deep learning architecture for classifying HEA microstructures. (B) Comparison of test accuracy in relation to the number of parameters. The area of the circles is proportional to the ratio of the test accuracy to the number of parameters in the model. (C) The confusion matrix demonstrates the predictive capabilities of the DenseNet-based model on the test dataset, showing over 95% accuracy for all categories except the eutectic + dendritic class, where the accuracy was lower. Reproduced with permission from Ref. [150]. Copyright 2021, Elsevier. (D) Modeling framework for predicting element distribution in PtNiPdCoFe HEAs, where DFT and evolutionary approach generate atomic models and simulated images to train a deep learning model that maps atomic column heights for each element via semantic segmentation. (E) Prediction of atomic column heights for each chemical element performed by the DL model applied to a simulated HAADF–STEM image randomly selected from the dataset. The predicted column heights (CHs) for Pt, Ni, Pd, Co, and Fe, along with the true values and R^2 values, indicate the goodness of fit. Pt and Pd exhibited the highest R^2 values calculated between the predicted and true heights. (F) Prediction results of the DL model applied to an experimental HAADF–STEM image of a PtNiPdCoFe HEA, showing the predicted atomic fractions of the five elements within the central region columns. Reproduced with permission from Ref. [164]. Copyright 2022, Elsevier.

element distribution in HEAs using scanning transmission electron microscopy (STEM) images, as illustrated in Figure 14D. Their work focused on PtNiPdCoFe HEAs, aiming to correlate the pixel intensities in STEM images with the number of atoms of various elements in atomic columns through semantic segmentation. The dataset comprised 10,000 simulated high-angle annular dark-field (HAADF) STEM images generated from realistic atomic models derived from DFT and evolutionary algorithm (EA) calculations, along with the corresponding ground truth data for training and testing the model. The FCN was trained to predict the column heights (CHs) for each element, achieving a maximum error of three atoms for most of the columns, with the majority of predictions accurate to within one atom. This high accuracy is illustrated in Figure 14E, which shows the predicted column heights for Pt, Ni, Pd, Co, and Fe, alongside the true values and R^2 values, indicating the goodness of fit. When applied to experimental HAADF–STEM images, the model successfully captured the irregular fluctuations and local aggregations of elements within the columns, particularly for Pt, which exhibited the most notable local aggregations with atomic fractions reaching up to 60% (Figure 14F). This study demonstrates the potential of deep learning in providing detailed insights into the atomic-scale distribution of elements in HEAs, offering valuable information on their structural properties and guiding future material design.

In addition to automated microstructure analysis, ML techniques can facilitate inverse material design by linking microstructural images with chemical compositions and mechanical properties [165]. Pei et al. [165] developed an ML framework to differentiate between morphologically similar martensitic and ferritic steels using 621 SEM images from 27 samples. This method utilized a variational autoencoder (VAE) combined with a regression model (Figure 15) to map high-dimensional image data into a low-dimensional latent space, effectively identifying subtle distinctions and emphasizing key elements such as Fe, Mn, B, and N. Expanding on this, the authors reversed the regression model's flow to create a “designer” network capable of deducing alloy compositions from desired microstructural characteristics, achieving the complex task of inverse design of alloys. This approach presents a promising and transferable framework for expediting the discovery of HEAs while minimizing experimental effort and cost.

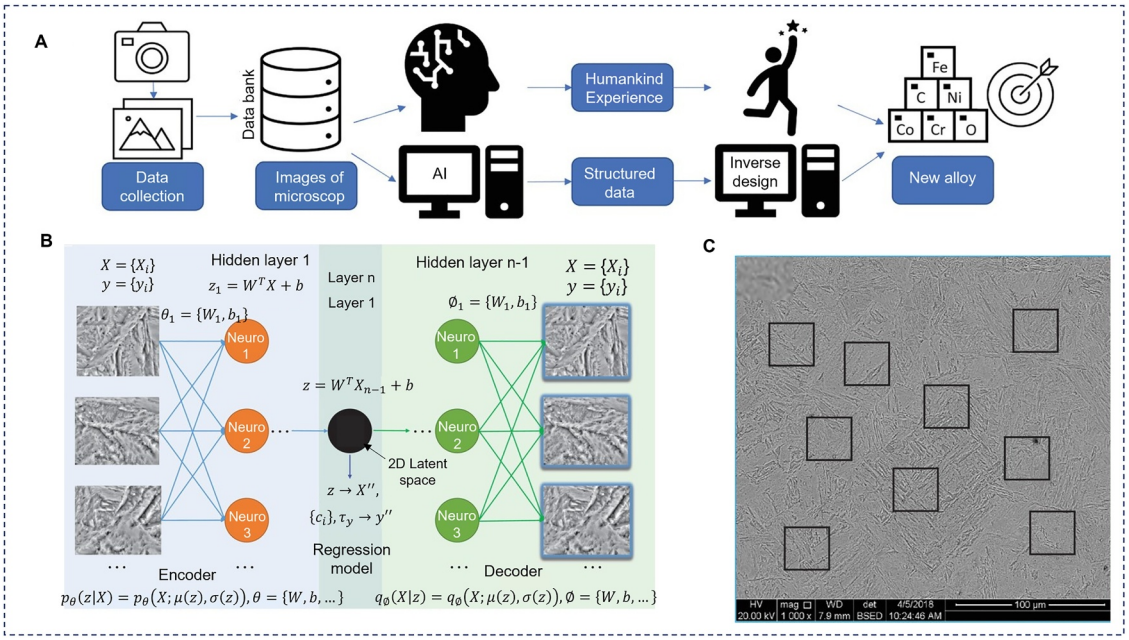

FIGURE 15 | Machine learning enables inverse material design by connecting microstructural images to alloy compositions, facilitating data-driven discovery of HEAs. (A) An overview comparison of material design approaches with and without artificial intelligence (AI). Conventional methods depend largely on human expertise and intuition, whereas AI introduces data-driven approaches that reduce the risk of bias and human error. (B) Random extraction of thirty-two 128 × 128-pixel subimages from a representative SEM image of the martensitic microstructure. (C) Schematic illustration of the ML model, VAE, used in this study, which comprises three main components: an encoder, a decoder, and a regression model. The regression model predicts alloy compositions critical for the subsequent inverse design process. During training, images are used as both inputs and targets, aiming to minimize the reconstruction error between input and output images. Reproduced with permission from Ref. [165]. Copyright 2021, the authors.

2.4 | Process Parameter Optimization

Various fabrication techniques have been employed to synthesize HEAs, such as vacuum arc melting (VAM), spark plasma sintering (SPS), magnetron sputtering deposition, thermal spraying, laser cladding, and selective laser melting (SLM). VAM, as shown in Figure 16, is the most common method for synthesizing HEAs. It involves melting metals in a sealed vacuum chamber filled with high-purity argon to prevent oxidation. A tungsten electrode generates an arc to melt the metal, and multiple remelting cycles ensure complete homogeneity of the melt [166]. SPS is a rapid consolidation technique that uses pulsed direct current and uniaxial pressure (25–150 MPa) to sinter powders, facilitating the fabrication of dense HEAs from powders at relatively low temperatures and short processing times. This technique enhances densification, reduces porosity, and refines the microstructure, thereby improving the mechanical properties of HEAs [167]. Conversely, laser cladding is a surface modification method used to apply HEA coatings by melting a feedstock material with a high-energy laser beam onto a substrate, creating a strong metallurgical bond [168, 169]. HEA coatings produced using this method exhibit enhanced hardness, thermal stability, and excellent wear resistance [168, 170]. The SLM process has been used to fabricate complex HEA components by selectively melting metal powders in a layer-by-layer manner using a high-energy laser, with powder layer thicknesses typically ranging from 20 to 100 μm [171, 172]. The powder bed fusion technique allows precise geometric control and tailored microstructures, making it a valuable tool in advanced HEA manufacturing. These fabrication techniques vary in terms of processing conditions, compositional flexibility, and resulting properties.

To fabricate HEAs effectively, it is crucial to fine-tune the process parameters to achieve the desired microstructure, reduce defects such as porosity and cracking, and obtain the desired mechanical properties. Poor control over these parameters can compromise the performance and reliability of the parts. Typically, optimization involves a combination of experimental trials and computational modeling to determine the optimal parameter sets [173–175]. In situ monitoring and postprocess testing further enhance process refinement. Although experimental trials are straightforward and intuitive to implement for exploring process behavior, they can be time-consuming and inefficient when multiple parameters and their interactions need to be evaluated simultaneously. Conversely, computational modeling provides a robust method for simulating and predicting the effects of process parameters, thereby reducing the need for extensive physical trials. Vogiatzief et al. [173] employed response surface methodology (RSM) to systematically optimize laser power, scanning speed, and hatch spacing in the laser powder bed fusion of $Al_{0.9}Cr_{0.9}Fe_{2.1}Ni_{2.1}$ HEA. RSM combines experimental and computational techniques—in this case, the Box–Behnken design and fitting a quadratic model to experimental data. Lin et al. [174, 175] applied polynomial regression modeling to optimize the SLM process parameters for a FeCoCrNi HEA, resulting in an almost fully dense material (99.78%) with enhanced mechanical properties, including a yield strength of 701 MPa, tensile strength of 907 MPa, and elongation at fracture of 30.8% [174].

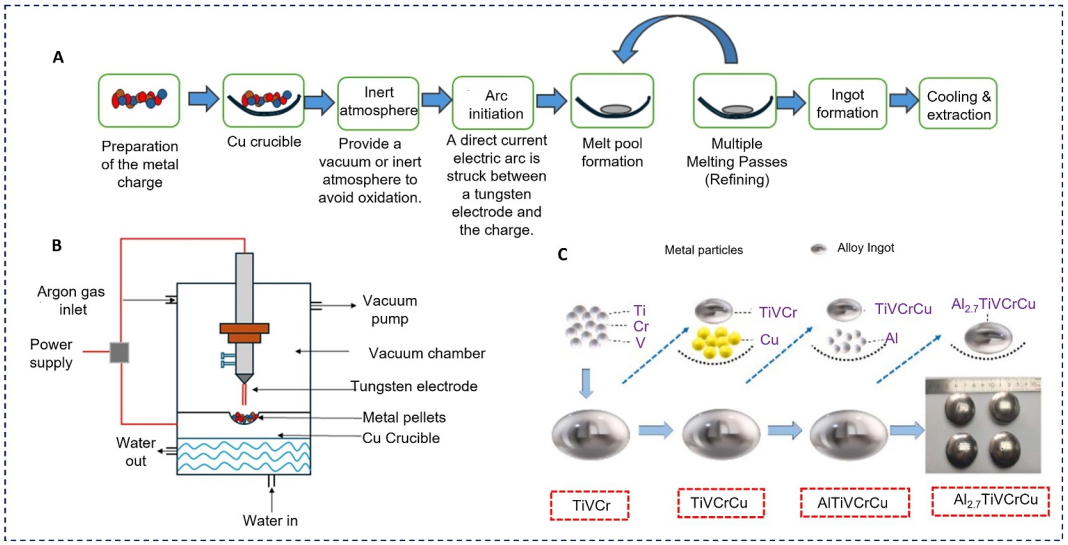

FIGURE 16 | An overview of the vacuum arc melting (VAM) process for the synthesis of HEAs. (A) VAM flow process, (B) schematic of VAM method, and (C) schematic of multistage VAM of a lightweight (density ~4.97 g cm^{-3}) $Al_{2.7}TiVCrCu$ HEA. Reproduced with permission from Ref. [166]. Copyright 2023, Elsevier.

ML is adept at capturing complex, nonlinear, and high-dimensional interactions among process parameters and outcomes, often with greater predictive accuracy. Its scalability, generalization capabilities, and support for real-time automated optimization make it particularly suitable for dynamic material processing environments. In additive manufacturing (AM), ML effectively addresses challenges such as the interdependence and nonlinearity of process parameters, including power, scan speed, layer thickness, and hatch spacing [176, 177]. Rankouhi et al. [176] employed a multivariate Gaussian process regression model to optimize process parameters in the SLM of 316L-Cu multi-material parts. By leveraging high-throughput experimental data on density and surface roughness, the model predicted the optimal laser power, scan speed, and hatch spacing for different alloy compositions. Park et al. [177] developed an ML-based optimization system for SLM to improve the quality of Ti–6Al–4V parts for biomedical applications. The authors used a deep neural network to correlate four key process parameters (laser power, laser scanning speed, layer thickness, and hatch distance) with the part density ratio and surface roughness. The model, trained on 2048 data points, achieved an R^2 value of 99%, demonstrating high accuracy. In addition, a graphical user interface (GUI) was developed to facilitate parameter selection and enhance user convenience. Thus, ML has the potential to reduce the need for numerous costly trial-and-error experiments, which often result in cumbersome and inefficient process parameter optimization and limited accuracy.

The integration of ML into the optimization of process parameters for HEAs is still in its early stages. Wang et al. [178] proposed a dimensionally augmented and physics-informed ML method to predict and optimize the process parameters of SLM for fabricating CoCrFeNiMn HEA components. This study employed a dataset comprising 110 samples created under systematically varied process parameters: laser power, hatching space, scanning speed, and layer thickness. Based on this dataset, the researchers trained four ML models, including ANN, Bayesian network (BN), SVM, and RF, to predict critical AM quality metrics: surface roughness and relative density. Feature engineering expanded the original 4-dimensional parameter set into a 206-dimensional space, whereas domain-specific physical features, such as peak melt pool temperature and Marangoni flow, were integrated to enhance model performance (Figure 17A) for the modeling strategy framework. The study assessed the predicted and experimental results using R^2, mean squared error (MSE), and mean absolute percentage error (MAPE) to evaluate the four ML strategies for top-layer surface roughness and relative density, as shown in Figure 17B,C, respectively. SVM consistently demonstrated the highest prediction accuracy and generalization, with the best outcomes achieved by a dimensionally augmented and physics-informed model. This study demonstrates that ML models not only improve the prediction fidelity of HEAs but also provide practical guidance for optimizing SLM parameters, thereby minimizing costly trial-and-error processes and enhancing material processing efficiency and quality.

To accurately predict the mechanical properties of alloys, both their composition and postprocessing parameters must be taken into account. Relying solely on composition overlooks the microstructural alterations caused by fabrication processes, resulting in unreliable predictions of properties, such as yield strength. Bajpai et al. [179] developed a residual ensemble learning model (RELM), a hybrid ML framework combining RF and gradient boosting regressors, trained on a dataset of 543 CoCrFeMnNi-based FCC HEAs (Figure 18A). The model incorporates both compositional features and critical processing parameters, such as annealing temperature, annealing time, and degree of plastic deformation, all of which significantly influence dislocation density and grain structure. To improve the model's fidelity and interpretability, physics-informed descriptors such as elastic modulus, lattice distortion, and mixing entropy were incorporated. RELM demonstrated high predictive accuracy (R^2 = 0.915) and outperformed traditional models (Figure 18B). As shown in Figure 18C, feature importance analyses using SHAP and partial dependence plots identified processing parameters, especially annealing temperature and

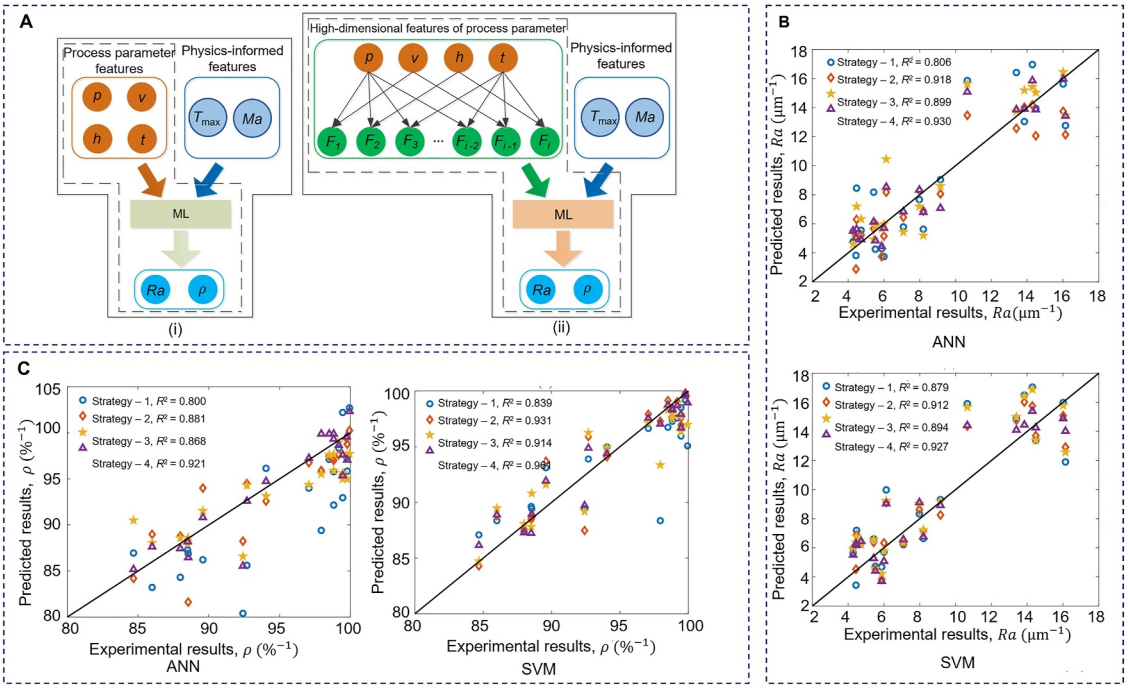

FIGURE 17 | ML-driven optimization of SLM process parameters for HEAs, integrating feature engineering and physics-informed inputs to improve part quality. (A) Schematic of the four strategies for predicting the quality characteristics of AM CoCrFeNiMn HEA parts. (i) Models based on the original process parameters, with and without the integration of physics-informed features. (ii) Models using dimensionally augmented features derived through nonlinear combinations of the original parameters, with and without physics-informed inputs. The solid lines represent models incorporating physics-based information, whereas the dotted lines represent models without it. Comparison of predicted and experimental values for (B) top-layer surface roughness and (C) relative density of CoCrFeNiMn HEA samples using two ML models: ANN and SVM. Each model was evaluated using four strategies: Strategy 1, the original process parameters; Strategy 2, dimensionally augmented features via feature engineering; Strategy 3, original features combined with physics-informed inputs; and Strategy 4, a hybrid of dimensional augmentation and physics-informed features. Reproduced with permission from Ref. [178]. Copyright 2022, Elsevier.

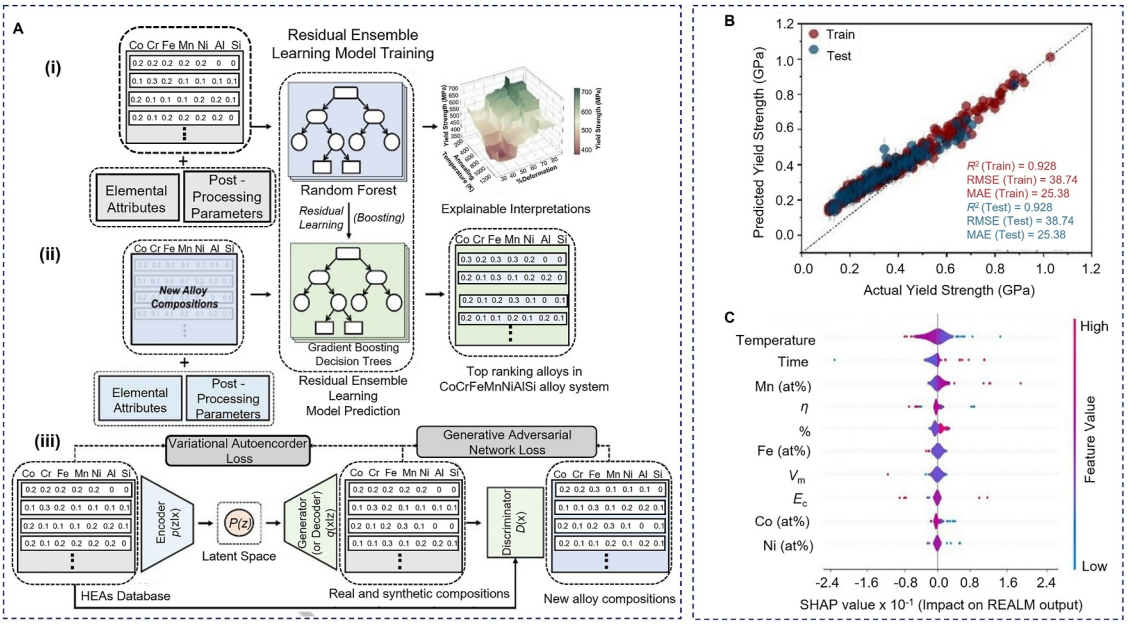

FIGURE 18 | Integration of compositional features and processing parameters in the residual ensemble learning model (RELM) to predict and optimize the yield strength of CoCrFeMnNi-based FCC HEAs. (A) Workflow of the RELM framework for targeted FCC HEA design: (i) RELM development and training using diverse feature spaces (over 10 seeds), enabling interpretation of composition–processing–property relationships; (ii) yield strength prediction using the mean output from 10 RELM models, with variance representing prediction uncertainty; and (iii) novel composition generation using a GAN–VAE hybrid model. (B) Parity plot illustrating predicted versus experimental yield strength for CoCrFeMnNi FCC HEAs with high predictive accuracy (R^2 = 0.915). (C) Feature importance ranked by mean absolute SHAP values of key factors affecting FCC HEA yield strength. Reproduced with permission from Ref. [179]. Copyright 2024, the authors.

time, as the most influential factors in determining yield strength. The model further guided the design and optimization of two new HEAs, $Co_{20}Cr_{16}Fe_{20}Mn_{16}Ni_{24}Al_4$ and $Co_{24}Cr_{12}Fe_{12}Mn_{16}Ni_{28}Al_4Si_4$, which achieved experimentally validated yield strengths of 842 and 937 MPa, respectively. This study emphasizes the importance of integrating postfabrication parameters into data-driven alloy design and highlights the potential of the RELM as both a predictive and interpretive tool for optimizing processing conditions in HEAs.

3 | Challenges and Future Directions

3.1 | Limitations of Data-Driven Approaches

ML leverages mathematical and statistical models to efficiently analyze large datasets, facilitating the discovery of new materials. By capturing complex nonlinear correlations between input parameters and process outcomes, ML enhances the understanding of the process–structure–property paradigm in HEAs. However, ML faces numerous challenges. The successful application of ML in the study and design of materials heavily depends on the availability of high-quality and extensive datasets. Often, data for ML are collected under varying experimental conditions, necessitating meticulous calibration to maintain consistency and reliability when integrating these datasets. Moreover, generating experimental data for HEAs is resource-intensive, time-consuming, and subject to variability. This challenge is exacerbated under extreme conditions, such as high temperatures or pressures, where experimental data are limited. These challenges impede the development of comprehensive and reliable datasets, thus limiting the accuracy and generalizability of ML models in HEA studies. When datasets are limited, simpler ML models, such as linear regression and SVM, often perform better than more complex approaches, such as NNs, which are prone to overfitting owing to their high data requirements [5, 133, 147, 180]. Overfitting occurs when a model learns the training data too precisely, including their noise or irregularities, which hampers its ability to accurately predict outcomes on new, unseen data. The quality and diversity of research data are thus vital for effective ML in the field of materials science. For example, Islam et al. [147] reported that their ML model for phase prediction was constrained by the small size of the dataset, resulting in an accuracy that was lower than expected when cross-validated, revealing the potential for overfitting. Sharing both successful and "failed" experimental results is essential, as negative data contribute to more balanced datasets and improve the robustness of the model [139]. To maximize their impact, these results should be openly published (in an open data repository for HEAs) in standardized and interoperable formats, thereby facilitating broader accessibility and integration across the research community.

Interpretability remains a significant challenge in applying ML models to HEAs [106, 117, 133, 181]. ML models such as NN function as "black boxes," offering limited insight into how predictions are made [180]. This lack of transparency poses issues in materials research, where understanding the underlying physical mechanisms behind material properties is essential for guiding experimental efforts and informing the design of new alloys. Without transparent models, converting predictive results into practical scientific knowledge becomes a challenging task. In addition, the difficulty in quantitatively assessing prediction uncertainty is a notable issue. Uncertainties may arise from model selection, sparse data, and noisy experimental observations. HEAs also present challenges in feature extraction and representation owing to the lack of regularity in their structures. Unlike ordered alloy systems, in which periodicity and symmetry allow for simpler and more efficient descriptors, disordered alloy systems require more complex representations. These are computationally demanding and may fail to capture the key properties that dictate material performance. Techniques such as ensemble learning and hyperparameter tuning can improve model accuracy but are also often computationally intensive, particularly when dealing with high-dimensional data from HEAs.

3.2 | Emerging Technical Breakthroughs

Integrating other computational techniques with ML offers a promising approach to tackling the issue of limited data in HEA research [152, 154, 164, 182]. High-fidelity simulations, such as first-principles and MD, can generate detailed data on microstructural evolution and mechanical properties, whereas CALPHAD simulations provide insights into phase transformations. These methods collectively create a more comprehensive and data-rich framework for designing and optimizing HEAs. Moreover, ML models, such as generative adversarial networks (GANs), have become powerful tools for addressing data scarcity in ML applications for HEAs [5, 148, 153]. By employing an adversarial training process between a generator and a discriminator, GANs can synthesize realistic and diverse data samples that augment the limited experimental datasets available for HEAs, thereby improving the robustness and generalization of predictive models. Additionally, transfer learning enables ML models initially trained on large datasets from related alloy systems, such as ordered alloy systems, to be adapted for HEAs, thereby significantly reducing the need for large labeled datasets specific to the target HEA. Although these methods only offer partial solutions, they have not yet completely addressed the limited data challenge in HEA research. As ML models become increasingly complex, building high-quality, well-curated datasets is crucial for their effective training and application. Even with large datasets, NNs are still prone to overfitting, making careful design essential. Strategies to mitigate overfitting in NN include regularization, thoughtful neural architecture design and parameter sharing, early stopping, balancing network breadth and depth, and employing ensemble methods [5, 23, 136, 180].

Advancing interpretable ML algorithms is an essential step toward uncovering the underlying physical mechanisms within these models. Methods such as local interpretable model-agnostic explanation (LIME) and SHapley Additive exPlanations (SHAP) assess the impact of each input feature on a given prediction, thereby offering insights into how compositional or processing variables influence material properties [5, 156, 179, 183]. Furthermore, the integration of domain knowledge through physics-informed ML helps ground model behavior in established

scientific principles, thereby enhancing the transparency and reliability of the predictions [178, 184]. Uncertainty quantification (UQ) has become a crucial tool for detecting bias in predictions by evaluating the model's confidence in its outputs. An emerging UQ method is an evidence-based recommender system (ERS) for HEAs, which leverages Dempster–Shafer (DS) theory, a generalization of the Bayesian method designed to manage incomplete information and imperfect data [185]. UQ is essential in inverse material design because it prevents overconfidence in predictions, guides experimental prioritization, and helps researchers distinguish between recommendations and speculative assumptions.

3.3 | Interdisciplinary Opportunities for ML in HEAs

ML presents transformative interdisciplinary opportunities for the exploration and advancement of HEAs, which are known for their compositional complexity and exceptional performance in diverse environments. Although considerable advancements have been made, opportunities still exist to expand the use of ML in HEA research. Realizing this potential will require deeper interdisciplinary collaboration, combining expertise in materials science, physics, chemistry, computer science, and data science, as illustrated in Figure 19.

One significant area for progress is the use of ML-driven high-throughput characterization and data acquisition. Relying on expert knowledge to manually extract information from vast quantities of scientific data is time-consuming and inefficient. This underscores the growing demand for rapid and precise automated data extraction techniques to streamline the process and support large-scale materials informatics. The integration of ML with high-throughput characterization techniques has the potential to revolutionize HEA research. ML algorithms can rapidly analyze intricate HEA datasets generated by advanced characterization tools, such as X-ray diffraction, electron microscopy, and spectroscopy, thereby enabling the faster identification of structure–property relationships. When integrated with automated data acquisition and processing systems, ML can efficiently screen extensive compositional spaces, significantly reducing experimental time and costs. This synergy not only enhances the reliability of data-driven models but also facilitates the development of predictive frameworks to inform HEA design.

There is also significant potential for applying ML to the discovery of HEAs for energy storage and conversion. By integrating ML with high-throughput experimentation and computational modeling, the process of designing alloys specifically for use in batteries, supercapacitors, and electrocatalysis can be made more efficient. Future research could expand the application of data-driven methods to accelerate the identification of stable, high-performance materials for advanced energy systems, thereby minimizing reliance on trial-and-error techniques and fostering the development of more environmentally friendly and sustainable technologies. At the same time, practical challenges, such as material costs, availability, and density, impose significant limitations that future ML models should increasingly consider. Many promising HEAs optimized by ML currently contain rare or costly elements, which restricts their commercial potential. There is an expanding opportunity to develop ML models that strike a balance between performance, cost, and environmental factors, aiding in the discovery of affordable HEAs that are suitable for catalysis or lightweight for structural applications in the aerospace industry.

Another promising direction involves the use of ML in the autonomous processing and fabrication of HEAs. In material processing, ML aids in fine-tuning parameters, such as heat treatment or settings for additive manufacturing, allowing for

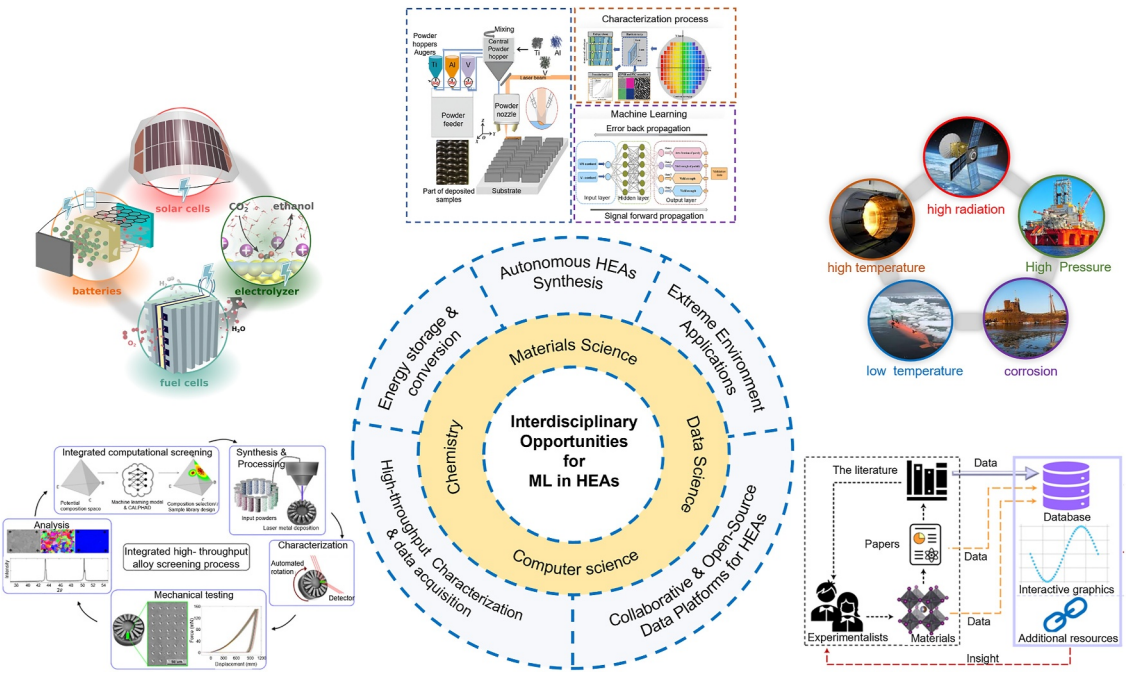

FIGURE 19 | Interdisciplinary opportunities for ML in HEAs [186–188].

more precise control over the microstructure and properties. This capability is further enhanced by active learning and Bayesian optimization, which significantly improve iterative fabrication processes. Active learning identifies the most informative data points, whereas Bayesian optimization employs probabilistic models to guide experiments toward optimal designs with fewer trials. When combined with robotic systems, these techniques facilitate automated synthesis and evaluation, enabling fast, data-driven decisions regarding the next promising material candidate to test, thereby accelerating the discovery of new materials.

Furthermore, ML is poised to significantly influence the advancement of HEAs for use in extreme environments characterized by high pressure, elevated temperatures, cryogenic conditions, corrosive elements, and intense radiation. Because of their exceptional properties and phase stability, future research on HEAs could focus on expanding datasets that capture their behavior under such harsh conditions, enabling ML models to predict their long-term performance and inform the design of alloys. To fully harness the capabilities of ML in HEA research, it is essential to develop standardized, open-access data platforms that merge experimental and simulation datasets from different fields. Such platforms can boost reproducibility, enhance model generalization, and accelerate scientific discoveries. As ML tools and data infrastructure continue to evolve, their capacity to tackle the complexities of HEAs will expand, establishing ML as a pivotal force in the future of alloy design and development.

4 | Conclusions

HEAs represent a paradigm shift in alloy design, offering compositional flexibility and exceptional properties. The development of HEAs has evolved considerably, from traditional methods to the integration of ML techniques. Although experimental and conventional computational methods have laid the groundwork for understanding HEA behavior, their relative limitations in scalability and efficiency have become more apparent in complex HEA designs. ML has emerged as a powerful alternative, enabling the rapid exploration of vast compositional design spaces, the prediction of material properties, and the optimization of processing conditions with accuracy. However, the successful implementation of ML in HEA research necessitates overcoming challenges such as data scarcity, model interpretability, and uncertainty quantification. Efforts have been made to tackle these issues, including data augmentation, transfer learning, and generative adversarial networks (GANs), to synthetically expand the available datasets. Techniques such as SHAP and LIME, along with physics-informed approaches, have been employed to address model interpretability, whereas techniques based on the Bayesian method have been tested to manage uncertainty quantification. Looking forward, the future of HEA design hinges on the following aspects:

1. Seamless integration of high-throughput computational data: Techniques such as DFT and CALPHAD-based thermodynamic simulations generate vast amounts of data that can form the basis for ML models, addressing data scarcity. ML models can not only learn from these data but also ensure that their predictions are grounded in fundamental physical principles.
2. Advanced ML models, such as deep learning frameworks, including convolutional neural networks (CNNs), have demonstrated their effectiveness in handling the complex high-dimensional data characteristics of HEA systems. These models can identify complex nonlinear correlations that are otherwise difficult to capture using traditional methods, thereby aiding researchers in exploring an extensive design space with greater accuracy. As data complexity increases, the roles of transfer learning and active learning have become increasingly crucial. Transfer learning allows models to leverage knowledge from one alloy system to another, thereby enhancing their performance in scenarios with limited data. Conversely, active learning strategically selects the most informative data points for experimentation, minimizing the need for exhaustive trial-and-error testing and focusing experimental efforts where they are most impactful.
3. Automated data-driven high-throughput experimental techniques: By incorporating automated systems for data collection during experiments and employing real-time data analysis using ML, the materials discovery process can be significantly accelerated. This approach enables immediate feedback and adjustments to the experimental setup based on the predictions of the ML model.
4. Multiobjective optimization: This is crucial for the development of next-generation alloys, as it involves the simultaneous optimization of multiple, often competing material properties, such as strength and ductility. Additionally, frameworks for multiobjective optimization should facilitate alloy design that considers not only material properties but also factors such as cost, environmental impact, and recyclability, thereby aligning with both industrial and sustainability goals. Consequently, ML models that integrate multiobjective optimization techniques will be adept at balancing these trade-offs and identifying alloy compositions that fulfill complex performance targets.
5. Collaborative and open-source platforms: Establishing collaborative, open-source platforms that facilitate the sharing of HEA experimental and computational data, along with offering specialized ML tools for HEA design, will significantly accelerate material discovery.

Author Contributions

Chrispin Ouko Zamzu: conceptualization, data curation, investigation, methodology, visualization, writing – original draft. **Zhe Jia:** conceptualization, funding acquisition, supervision, validation, writing – review and editing. **Baolong Shen:** conceptualization, funding acquisition, supervision, validation, writing – review and editing.

Acknowledgments

This work was financially supported by the National Natural Science Foundation of China (Grant Nos. 52201174, 52571182, and 52231005), the Natural Science Foundation of Jiangsu Province (Grant Nos. BK20220858 and BK20253026), the Start-up Research Fund of Southeast University

(Grant No. RF1028623100), and the Fundamental Research Funds for the Central Universities (Grant Nos. 2242023K5001 and 2242023K40029).

Conflicts of Interest

Zhe Jia is an editorial board member for Rare Metals and was not involved in the editorial review or the decision to publish this article. All authors declare that there are no competing interests.

Data Availability Statement

The data that support the findings of this study are available from the corresponding author upon reasonable request.

References

1. J. W. Yeh, S. K. Chen, S. J. Lin, et al., "Nanostructured High-Entropy Alloys With Multiple Principal Elements: Novel Alloy Design Concepts and Outcomes," *Advanced Engineering Materials* 6, no. 5 (2004): 299–303, https://doi.org/10.1002/adem.200300567.

2. B. Cantor, I. T. H. Chang, P. Knight, and A. J. B. Vincent, "Microstructural Development in Equiatomic Multicomponent Alloys," *Materials Science and Engineering A* 375–377 (2004): 213–218, https://doi.org/10.1016/j.msea.2003.10.257.

3. B. Zhang, Y. Zhang, and S. Guo, "A Thermodynamic Study of Corrosion Behaviors for CoCrFeNi-Based High-Entropy Alloys," *Journal of Materials Science* 53, no. 20 (2018): 14729–14738, https://doi.org/10.1007/s10853-018-2652-2.

4. R. Li, L. Xie, W. Y. Wang, P. K. Liaw, and Y. Zhang, "High-Throughput Calculations for High-Entropy Alloys: A Brief Review," *Frontiers in Materials* 7 (2020): 290, https://doi.org/10.3389/fmats.2020.00290.

5. S. Wu, Z. Song, J. Wang, X. Niu, and H. Chen, "Enhanced Phase Prediction of High-Entropy Alloys Through Machine Learning and Data Augmentation," *Physical Chemistry Chemical Physics* 27, no. 2 (2024): 717–729, https://doi.org/10.1039/d4cp04496g.

6. E. W. Huang, W. J. Lee, S. S. Singh, et al., "Machine-Learning and High-Throughput Studies for High-Entropy Materials," *Materials Science and Engineering: R: Reports* 147 (2022): 100645, https://doi.org/10.1016/j.mser.2021.100645.

7. W. Huang, P. Martin, and H. L. Zhuang, "Machine-Learning Phase Prediction of High-Entropy Alloys," *Acta Materialia* 169 (2019): 225–236, https://doi.org/10.1016/j.actamat.2019.03.012.

8. X. Wang, W. Guo, and Y. Fu, "High-Entropy Alloys: Emerging Materials for Advanced Functional Applications," *Journal of Materials Chemistry A* 9, no. 2 (2021): 663–701, https://doi.org/10.1039/d0ta09601f.

9. J. W. Yeh, "Alloy Design Strategies and Future Trends in High-Entropy Alloys," *JOM* 65, no. 12 (2013): 1759–1771, https://doi.org/10.1007/s11837-013-0761-6.

10. D. B. Miracle and O. N. Senkov, "A Critical Review of High Entropy Alloys and Related Concepts," *Acta Materialia* 122 (2017): 448–511, https://doi.org/10.1016/j.actamat.2016.08.081.

11. Y. Zhang, Y. J. Zhou, J. P. Lin, G. L. Chen, and P. K. Liaw, "Solid-Solution Phase Formation Rules for Multi-Component Alloys," *Advanced Engineering Materials* 10, no. 6 (2008): 534–538, https://doi.org/10.1002/adem.200700240.

12. D. B. Miracle, J. D. Miller, O. N. Senkov, C. Woodward, M. D. Uchic, and J. Tiley, "Exploration and Development of High Entropy Alloys for Structural Applications," *Entropy* 16, no. 1 (2014): 494–525, https://doi.org/10.3390/e16010494.

13. F. Otto, Y. Yang, H. Bei, and E. P. George, "Relative Effects of Enthalpy and Entropy on the Phase Stability of Equiatomic High-Entropy Alloys," *Acta Materialia* 61, no. 7 (2013): 2628–2638, https://doi.org/10.1016/j.actamat.2013.01.042.

14. S. Guo and C. T. Liu, "Phase Stability in High Entropy Alloys: Formation of Solid-Solution Phase or Amorphous Phase," *Progress in Natural Science: Materials International* 21, no. 6 (2011): 433–446, https://doi.org/10.1016/s1002-0071(12)60080-x.

15. X. Yang and Y. Zhang, "Prediction of High-Entropy Stabilized Solid-Solution in Multi-Component Alloys," *Materials Chemistry and Physics* 132, no. 2–3 (2012): 233–238, https://doi.org/10.1016/j.matchemphys.2011.11.021.

16. H. W. Luan, Y. Shao, J. F. Li, et al., "Phase Stabilities of High Entropy Alloys," *Scripta Materialia* 179 (2020): 40–44, https://doi.org/10.1016/j.scriptamat.2019.12.041.

17. C. Ng, S. Guo, J. Luan, S. Shi, and C. T. Liu, "Entropy-Driven Phase Stability and Slow Diffusion Kinetics in an $Al_{0.5}$CoCrCuFeNi High Entropy Alloy," *Intermetallics* 31 (2012): 165–172, https://doi.org/10.1016/j.intermet.2012.07.001.

18. X. W. Yang, X. H. Shi, H. J. Yang, J. W. Qiao, P. K. Liaw, and Y. C. Wu, "Entropy Versus Enthalpy in Hexagonal-Close-Packed High-Entropy Alloys," *Rare Metals* 41, no. 8 (2022): 2906–2920, https://doi.org/10.1007/s12598-022-02010-4.

19. C. Y. Cheng, Y. C. Yang, Y. Z. Zhong, Y. Y. Chen, T. Hsu, and J. W. Yeh, "Physical Metallurgy of Concentrated Solid Solutions From Low-Entropy to High-Entropy Alloys," *Current Opinion in Solid State & Materials Science* 21, no. 6 (2017): 299–311, https://doi.org/10.1016/j.cossms.2017.09.002.

20. K. Y. Tsai, M. H. Tsai, and J. W. Yeh, "Sluggish Diffusion in Co-Cr-Fe-Mn-Ni High-Entropy Alloys," *Acta Materialia* 61, no. 13 (2013): 4887–4897, https://doi.org/10.1016/j.actamat.2013.04.058.

21. J. Dąbrowa, W. Kucza, G. Cieślak, T. Kulik, M. Danielewski, and J. W. Yeh, "Interdiffusion in the FCC-Structured Al-Co-Cr-Fe-Ni High Entropy Alloys: Experimental Studies and Numerical Simulations," *Journal of Alloys and Compounds* 674 (2016): 455–462, https://doi.org/10.1016/j.jallcom.2016.03.046.

22. S. L. Thomas and S. Patala, "Vacancy Diffusion in Multi-Principal Element Alloys: The Role of Chemical Disorder in the Ordered Lattice," *Acta Materialia* 196 (2020): 144–153, https://doi.org/10.1016/j.actamat.2020.06.022.

23. P. I. Odetola, B. J. Babalola, A. E. Afolabi, et al., "Exploring High Entropy Alloys: A Review on Thermodynamic Design and Computational Modeling Strategies for Advanced Materials Applications," *Heliyon* 10, no. 22 (2024): e39660, https://doi.org/10.1016/j.heliyon.2024.e39660.

24. K. H. Lin, C. M. Tseng, C. C. Chueh, et al., "Different Lattice Distortion Effects on the Tensile Properties of Ni-W Dilute Solutions and CrFeNi and CoCrFeMnNi Concentrated Solutions," *Acta Materialia* 221 (2021): 117399, https://doi.org/10.1016/j.actamat.2021.117399.

25. Y. Tong, L. Bai, X. Liang, et al., "Influence of Alloying Elements on Mechanical and Electronic Properties of NbMoTaWX (X = Cr, Zr, V, Hf and Re) Refractory High Entropy Alloys," *Intermetallics* 126 (2020): 106928, https://doi.org/10.1016/j.intermet.2020.106928.

26. X. J. Gao, L. Wang, N. N. Guo, et al., "Microstructure Characteristics and Mechanical Properties of $Hf_{0.5}Mo_{0.5}$NbTiZr Refractory High Entropy Alloy With Cr Addition," *International Journal of Refractory Metals and Hard Materials* 95 (2021): 105405, https://doi.org/10.1016/j.ijrmhm.2020.105405.

27. J. Yang, M. Y. Zhou, and J. J. Yang, "Annealing-Induced Gradient Nanostructured FeCrAlTiMo High-Entropy Alloy Coatings With Significantly Enhanced Wear Resistance," *Tungsten* 6, no. 3 (2024): 544–548, https://doi.org/10.1007/s42864-023-00257-7.

28. B. X. Cao, C. Wang, T. Yang, and C. T. Liu, "Cocktail Effects in Understanding the Stability and Properties of Face-Centered-Cubic High-Entropy Alloys at Ambient and Cryogenic Temperatures," *Scripta Materialia* 187 (2020): 250–255, https://doi.org/10.1016/j.scriptamat.2020.06.008.

29. G. Laplanche, A. Kostka, C. Reinhart, J. Hunfeld, G. Eggeler, and E. P. George, "Reasons for the Superior Mechanical Properties of Medium-Entropy CrCoNi Compared to High-Entropy CrMnFeCoNi," *Acta Materialia* 128 (2017): 292–303, https://doi.org/10.1016/j.actamat.2017.02.036.

30. S. Huang, W. Li, S. Lu, et al., "Temperature Dependent Stacking Fault Energy of FeCrCoNiMn High Entropy Alloy," *Scripta Materialia* 108 (2015): 44–47, https://doi.org/10.1016/j.scriptamat.2015.05.041.

31. Z. Li, K. G. Pradeep, Y. Deng, D. Raabe, and C. C. Tasan, "Metastable High-Entropy Dual-Phase Alloys Overcome the Strength-Ductility Trade-Off," *Nature* 534, no. 7606 (2016): 227–230, https://doi.org/10.1038/nature17981.

32. H. W. Ma, Y. C. Zhao, L. Feng, et al., "Achieving Strength–Ductility Synergy in Novel Paramagnetic Fe-Based Medium-Entropy Alloys Through Deep Cryogenic Deformation," *Rare Metals* 43, no. 9 (2024): 4493–4507, https://doi.org/10.1007/s12598-024-02865-9.

33. S. Y. Liang, L. T. Zhang, Y. J. Wang, B. Wang, J. M. Pelletier, and J. C. Qiao, "A Model on the Coupling Between Cyclic Fatigue and Microstructure Evolution in a Metallic Glass," *International Journal of Fatigue* 187 (2024): 108446, https://doi.org/10.1016/j.ijfatigue.2024.108446.

34. R. S. Ganji, P. S. Karthik, K. B. S. Rao, and K. V. Rajulapati, "Strengthening Mechanisms in Equiatomic Ultrafine Grained AlCoCrCuFeNi High-Entropy Alloy Studied by Micro- and Nanoindentation Methods," *Acta Materialia* 125 (2017): 58, https://doi.org/10.1016/j.actamat.2016.11.046.

35. Y. F. Kao, T. J. Chen, S. K. Chen, and J. W. Yeh, "Microstructure and Mechanical Property of As-Cast, -Homogenized, and -Deformed $Al_xCoCrFeNi$ ($0 \le x \le 2$) High-Entropy Alloys," *Journal of Alloys and Compounds* 488, no. 1 (2009): 57–64, https://doi.org/10.1016/j.jallcom.2009.08.090.

36. P. Cheng, Y. Zhao, X. Xu, S. Wang, Y. Sun, and H. Hou, "Microstructural Evolution and Mechanical Properties of $Al_{0.3}CoCrFeNiSi_x$ High-Entropy Alloys Containing Coherent Nanometer-Scaled Precipitates," *Materials Science and Engineering A* 772 (2020): 138681, https://doi.org/10.1016/j.msea.2019.138681.

37. Y. G. Tong, N. Tian, H. F. Huang, et al., "Microstructure and Deformation Mechanism of Dual-Phase $Al_{0.5}CoCrNiFe$ High-Entropy Alloy," *Rare Metals* 42, no. 6 (2023): 2020–2027, https://doi.org/10.1007/s12598-022-02205-9.

38. H. T. Zhang, C. L. Wang, J. W. Miao, et al., "Effect of Microstructure Evolution on Wear Resistance of Equal Molar CoCrFeNi High-Entropy Alloy," *Rare Metals* 42, no. 11 (2023): 3797–3805, https://doi.org/10.1007/s12598-023-02384-z.

39. J. Lee, S. Kim, T. Kwon, et al., "Strengthening Mechanisms Analysis and Tailoring of Bimodal Grain Structures for Enhanced Strength in CoCrFeMnNi High-Entropy Alloys," *Rare Metals* 43, no. 8 (2024): 3893–3903, https://doi.org/10.1007/s12598-024-02799-2.

40. B. Gludovatz, A. Hohenwarter, D. Catoor, E. H. Chang, E. P. George, and R. O. Ritchie, "A Fracture-Resistant High-Entropy Alloy for Cryogenic Applications," *Science* 345, no. 6201 (2014): 1153–1158, https://doi.org/10.1126/science.1254581.

41. D. Li and Y. Zhang, "The Ultrahigh Charpy Impact Toughness of Forged $Al_xCoCrFeNi$ High Entropy Alloys at Room and Cryogenic Temperatures," *Intermetallics* 70 (2016): 24–28, https://doi.org/10.1016/j.intermet.2015.11.002.

42. S. Q. Xia, M. C. Gao, and Y. Zhang, "Abnormal Temperature Dependence of Impact Toughness in $Al_xCoCrFeNi$ System High Entropy Alloys," *Materials Chemistry and Physics* 210 (2018): 213–221, https://doi.org/10.1016/j.matchemphys.2017.06.021.

43. X. Fan, R. Qu, and Z. Zhang, "Relation Between Strength and Hardness of High-Entropy Alloys," *Acta Metallurgica Sinica* 34, no. 11 (2021): 1461–1482, https://doi.org/10.1007/s40195-021-01252-y.

44. E. Mak, B. Yin, and W. A. Curtin, "A Ductility Criterion for bcc High Entropy Alloys," *Journal of the Mechanics and Physics of Solids* 152 (2021): 104389, https://doi.org/10.1016/j.jmps.2021.104389.

45. X. Ding, Y. Zhan, and H. Tang, "Development of $CoCrFeNiVAl_x$ High-Entropy Alloys Based on Solid Solution Strengthening," *JOM* 71, no. 10 (2019): 3473–3480, https://doi.org/10.1007/s11837-019-03416-9.

46. V. Shivam, Y. Shadangi, J. Basu, and N. K. Mukhopadhyay, "Evolution of Phases, Hardness and Magnetic Properties of AlCoCrFeNi High Entropy Alloy Processed by Mechanical Alloying," *Journal of Alloys and Compounds* 832 (2020): 154826, https://doi.org/10.1016/j.jallcom.2020.154826.

47. H. Ren, R. R. Chen, X. F. Gao, et al., "A Hf-Doped Dual-Phase High-Entropy Alloy: Phase Evolution and Wear Features," *Rare Metals* 43, no. 1 (2024): 324–333, https://doi.org/10.1007/s12598-023-02410-0.

48. O. N. Senkov, J. M. Scott, S. V. Senkova, F. Meisenkothen, D. B. Miracle, and C. F. Woodward, "Microstructure and Elevated Temperature Properties of a Refractory TaNbHfZrTi Alloy," *Journal of Materials Science* 47, no. 9 (2012): 4062–4074, https://doi.org/10.1007/s10853-012-6260-2.

49. M. Xia, Y. Jiang, X. Yao, et al., "Mechanical Property and Improved Oxidation Resistance of Refractory High Entropy Alloy Fabricated by Laser Directed Energy Deposition," *Corrosion Science* 245 (2025): 112601, https://doi.org/10.1016/j.corsci.2024.112601.

50. B. Gorr, M. Azim, H. J. Christ, T. Mueller, D. Schliephake, and M. Heilmaier, "Phase Equilibria, Microstructure, and High Temperature Oxidation Resistance of Novel Refractory High-Entropy Alloys," *Journal of Alloys and Compounds* 624 (2015): 270–278, https://doi.org/10.1016/j.jallcom.2014.11.012.

51. Z. W. Li, B. X. Su, L. Wang, et al., "High Strength-Ductility Synergy in Refractory Multi-Principal Element Alloys via Special Deformation Mechanisms and Dislocation Behaviors," *Rare Metals* 44, no. 1 (2024): 608–622, https://doi.org/10.1007/s12598-024-02899-z.

52. S. L. Guo, W. Zhang, X. H. Yan, et al., "Developing Novel Ultra-Thin Refractory Medium-Entropy Foils With Excellent Strength-Ductility Synergy," *Rare Metals* 44, no. 2 (2024): 1380–1391, https://doi.org/10.1007/s12598-024-02910-7.

53. R. X. Wang, W. J. Shen, Y. J. Chen, et al., "Excellent Ductilization and Strengthening of Lightweight Refractory High-Entropy Alloys via Stable B2 Nanoprecipitates," *Rare Metals* 44, no. 3 (2024): 2128–2135, https://doi.org/10.1007/s12598-024-03032-w.

54. Y. Dilshodbek, S. H. Hong, M. A. Abbas, et al., "Evolution of Microstructure and Mechanical Characteristics of $(CrFeNiCu)_{100-x}Ti_x$ High-Entropy Alloys," *Rare Metals* 42, no. 9 (2023): 3088–3098, https://doi.org/10.1007/s12598-023-02286-0.

55. Y. Z. Yu, R. Y. Shi, Y. Zhang, et al., "Nanoprecipitate Improves High Strain-Rate Deformability in a High-Entropy Alloy," *Tungsten* 7, no. 2 (2025): 298–313, https://doi.org/10.1007/s42864-024-00295-9.

56. Y. Dong, Y. Lu, J. Kong, J. Zhang, and T. Li, "Microstructure and Mechanical Properties of Multi-Component $AlCrFeNiMo_x$ High-Entropy Alloys," *Journal of Alloys and Compounds* 573 (2013): 96–101, https://doi.org/10.1016/j.jallcom.2013.03.253.

57. C. Yang, J. Zhang, M. Li, and X. Liu, "Soft-Magnetic High-Entropy AlCoFeMnNi Alloys With Dual-Phase Microstructures Induced by Annealing," *Acta Metallurgica Sinica* 33, no. 8 (2020): 1124–1134, https://doi.org/10.1007/s40195-020-01086-0.

58. Y. X. Zhuang, X. L. Zhang, and X. Y. Gu, "Effect of Molybdenum on Phases, Microstructure and Mechanical Properties of $Al_{0.5}CoCrFeMo_xNi$ High Entropy Alloys," *Journal of Alloys and Compounds* 743 (2018): 514–522, https://doi.org/10.1016/j.jallcom.2018.02.003.

59. J. Kuang, P. Zhang, Q. Wang, Z. Hu, X. Liang, and B. Shen, "Formation and Oxidation Behavior of Refractory High-Entropy Silicide

(NbMoTaW)Si_2 Coating," *Corrosion Science* 198 (2022): 110134, https://doi.org/10.1016/j.corsci.2022.110134.

60. J. Kuang, Q. Wang, Z. Jia, et al., "Ablation-Resistant Yttrium-Modified High-Entropy Refractory Metal Silicide (NbMoTaW)Si_2 Coating for Oxidizing Environments Up To 2100°C," *Materials Today* 80 (2024): 156–166, https://doi.org/10.1016/j.mattod.2024.08.012.

61. L. B. Chen, R. Wei, K. Tang, et al., "Heavy Carbon Alloyed FCC-Structured High Entropy Alloy With Excellent Combination of Strength and Ductility," *Materials Science and Engineering A* 716 (2018): 150–156, https://doi.org/10.1016/j.msea.2018.01.045.

62. Z. X. Su, H. Y. Shi, Y. X. Bai, et al., "Oxygen-Driven Precipitate Evolution and Age-Softening Behavior in NbZrTi Refractory Multi-Principal Element Alloys," *Tungsten* (2025), https://doi.org/10.1007/s42864-025-00336-x.

63. Y. Wan, Y. Cheng, Y. Chen, et al., "A Nitride-Reinforced NbMoTaWHfN Refractory High-Entropy Alloy With Potential Ultra-High-Temperature Engineering Applications," *Engineering* 30 (2023): 110–120, https://doi.org/10.1016/j.eng.2023.06.008.

64. Q. Yu, S. Qiu, and Z. B. Jiao, "Atomic-Scale Understanding of Interstitial-Strengthened High-Entropy Alloys," *Rare Metals* 44, no. 9 (2025): 6002–6014, https://doi.org/10.1007/s12598-025-03358-z.

65. W. T. Zhang, X. Q. Wang, F. Q. Zhang, et al., "Frontiers in High Entropy Alloys and High Entropy Functional Materials," *Rare Metals* 43, no. 10 (2024): 4639–4776, https://doi.org/10.1007/s12598-024-02852-0.

66. C. Gu, J. H. Hu, J. B. Song, et al., "Effects of Ta Content on Microstructure and Oxidation Behavior of $AlCoCrFeNiYTa_x$ High Entropy Alloy," *Rare Metals* 43, no. 9 (2024): 4462–4475, https://doi.org/10.1007/s12598-024-02706-9.

67. S. Y. Liang, L. T. Zhang, B. Wang, et al., "Decoupling Thermal and Mechanical Effects on Metallic Glasses Creep," *International Journal of Mechanical Sciences* 302 (2025): 110573, https://doi.org/10.1016/j.ijmecsci.2025.110573.

68. L. Yang, S. Sen, D. Schliephake, et al., "Creep Behavior of a Precipitation-Strengthened A2-B2 Refractory High Entropy Alloy," *Acta Materialia* 288 (2025): 120827, https://doi.org/10.1016/j.actamat.2025.120827.

69. H. Ren, R. R. Chen, X. F. Gao, et al., "Introduction of Rare-Earth Element Sc in Alloy Design to Modify Wear Features of Dual-Phase High-Entropy Alloy," *Rare Metals* 43, no. 2 (2024): 817–828, https://doi.org/10.1007/s12598-023-02412-y.

70. E. Wakai, H. Noto, T. Shibayama, et al., "Microstructures and Hardness of BCC Phase Iron-Based High Entropy Alloy Fe-Mn-Cr-V-Al-C," *Materials Characterization* 211 (2024): 113881, https://doi.org/10.1016/j.matchar.2024.113881.

71. Q. Y. Cheng, M. F. Wang, J. J. Ni, et al., "High-Entropy Alloys for Accessing Hydrogen Economy via Sustainable Production of Fuels and Direct Application in Fuel Cells," *Rare Metals* 42, no. 11 (2023): 3553–3569, https://doi.org/10.1007/s12598-023-02343-8.

72. Y. Yao, Z. Huang, P. Xie, et al., "Carbothermal Shock Synthesis of High-Entropy-Alloy Nanoparticles," *Science* 359, no. 6383 (2018): 1489–1494, https://doi.org/10.1126/science.aan5412.

73. P. Xie, Y. Yao, Z. Huang, et al., "Highly Efficient Decomposition of Ammonia Using High-Entropy Alloy Catalysts," *Nature Communications* 10, no. 1 (2019): 4011, https://doi.org/10.1038/s41467-019-11848-9.

74. S. Nellaiappan, N. K. Katiyar, R. Kumar, et al., "High-Entropy Alloys as Catalysts for the CO_2 and CO Reduction Reactions: Experimental Realization," *ACS Catalysis* 10, no. 6 (2020): 3658–3663, https://doi.org/10.1021/acscatal.9b04302.

75. Z. Jia, T. Yang, L. Sun, et al., "A Novel Multinary Intermetallic as an Active Electrocatalyst for Hydrogen Evolution," *Advanced Materials* 32, no. 21 (2020): 2000385, https://doi.org/10.1002/adma.202000385.

76. H. Z. Hu, H. Q. Xiao, X. C. He, et al., "Development of Ti–V–Cr–Mn–Mo–Ce High-Entropy Alloys for High-Density Hydrogen Storage in Water Bath Environments," *Rare Metals* 43, no. 10 (2024): 5229–5241, https://doi.org/10.1007/s12598-024-02618-8.

77. Q. Wang, Y. Li, Y. Yang, et al., "Self-Supported AlFeNiCoMo High-Entropy Alloy With Micropillar Array Structure for Efficient Oxygen Evolution Reaction," *APL Materials* 10, no. 10 (2022): 101106, https://doi.org/10.1063/5.0117046.

78. Y. Yang, Z. Jia, X. Zhang, et al., "Chemical Short-Range Order in Multi-Principal Element Alloy With Ordering Effects on Water Electrolysis Performance," *Materials Today* 72 (2024): 97–108, https://doi.org/10.1016/j.mattod.2023.12.006.

79. Y. Yang, Z. Jia, Q. Wang, et al., "Vacancy Induced Microstrain in High-Entropy Alloy Film for Sustainable Hydrogen Production Under Universal pH Conditions," *Energy & Environmental Science* 17, no. 16 (2024): 5854–5865, https://doi.org/10.1039/d4ee01139b.

80. S. Y. Liang, F. Zhu, Y. J. Wang, et al., "On the Kinetics of Structural Evolution in Metallic Glasses," *International Journal of Engineering Science* 205 (2024): 104146, https://doi.org/10.1016/j.ijengsci.2024.104146.

81. Z. Jia, X. Duan, P. Qin, et al., "Disordered Atomic Packing Structure of Metallic Glass: Toward Ultrafast Hydroxyl Radicals Production Rate and Strong Electron Transfer Ability in Catalytic Performance," *Advanced Functional Materials* 27, no. 38 (2017): 1702258, https://doi.org/10.1002/adfm.201702258.

82. Z. Jia, J. Kang, W. C. Zhang, et al., "Surface Aging Behaviour of Fe-Based Amorphous Alloys as Catalysts During Heterogeneous Photo Fenton-Like Process for Water Treatment," *Applied Catalysis B: Environmental* 204 (2017): 537–547, https://doi.org/10.1016/j.apcatb.2016.12.001.

83. Z. Jia, Q. Wang, L. Sun, et al., "Attractive In Situ Self-Reconstructed Hierarchical Gradient Structure of Metallic Glass for High Efficiency and Remarkable Stability in Catalytic Performance," *Advanced Functional Materials* 29, no. 19 (2019): 1807857, https://doi.org/10.1002/adfm.201807857.

84. Z. Jia, W. C. Zhang, W. M. Wang, D. Habibi, and L. C. Zhang, "Amorphous $Fe_{78}Si_9B_{13}$ Alloy: An Efficient and Reusable Photo-Enhanced Fenton-Like Catalyst in Degradation of Cibacron Brilliant Red 3B-A Dye Under UV-Vis Light," *Applied Catalysis B: Environmental* 192 (2016): 46–56, https://doi.org/10.1016/j.apcatb.2016.03.048.

85. S. X. Liang, Z. Jia, W. C. Zhang, et al., "Ultrafast Activation Efficiency of Three Peroxides by $Fe_{78}Si_9B_{13}$ Metallic Glass Under Photo-Enhanced Catalytic Oxidation: A Comparative Study," *Applied Catalysis B: Environmental* 221 (2018): 108–118, https://doi.org/10.1016/j.apcatb.2017.09.007.

86. S. X. Liang, Z. Jia, Y. J. Liu, et al., "Compelling Rejuvenated Catalytic Performance in Metallic Glasses," *Advanced Materials* 30, no. 45 (2018): 1802764, https://doi.org/10.1002/adma.201802764.

87. L. C. Zhang, Z. Jia, F. Lyu, S. X. Liang, and J. Lu, "A Review of Catalytic Performance of Metallic Glasses in Wastewater Treatment: Recent Progress and Prospects," *Progress in Materials Science* 105 (2019): 100576, https://doi.org/10.1016/j.pmatsci.2019.100576.

88. Z. Jia, Y. Zhao, Q. Wang, et al., "Nanoscale Heterogeneities of Non-Noble Iron-Based Metallic Glasses Toward Efficient Water Oxidation at Industrial-Level Current Densities," *ACS Applied Materials & Interfaces* 14, no. 8 (2022): 10288–10297, https://doi.org/10.1021/acsami.1c22294.

89. S. X. Liang, Z. Jia, W. C. Zhang, W. M. Wang, and L. C. Zhang, "Rapid Malachite Green Degradation Using $Fe_{73.5}Si_{13.5}B_9Cu_1Nb_3$ Metallic Glass for Activation of Persulfate Under UV–Vis Light," *Materials & Design* 119 (2017): 244–253, https://doi.org/10.1016/j.matdes.2017.01.039.

90. Z. Jia, K. Nomoto, Q. Wang, et al., "A Self-Supported High-Entropy Metallic Glass With a Nanosponge Architecture for Efficient Hydrogen Evolution Under Alkaline and Acidic Conditions," *Advanced Functional*

Materials 31, no. 38 (2021): 2101586, https://doi.org/10.1002/adfm.202101586.

91. X. Zhang, Y. Yang, Y. Liu, et al., "Defect Engineering of a High-Entropy Metallic Glass Surface for High-Performance Overall Water Splitting at Ampere-Level Current Densities," *Advanced Functional Materials* 35, no. 38 (2023): 2303439, https://doi.org/10.1002/adma.202303439.

92. Z. Jia, Y. Yang, Q. Wang, et al., "An Ultrafast and Stable High-Entropy Metallic Glass Electrode for Alkaline Hydrogen Evolution Reaction," *ACS Materials Letters* 4, no. 8 (2022): 1389–1396, https://doi.org/10.1021/acsmaterialslett.2c00371.

93. Q. Wang, J. Li, Y. Li, G. Shao, Z. Jia, and B. Shen, "Non-Noble Metal-Based Amorphous High-Entropy Oxides as Efficient and Reliable Electrocatalysts for Oxygen Evolution Reaction," *Nano Research* 15, no. 10 (2022): 8751–8759, https://doi.org/10.1007/s12274-022-4179-8.

94. Q. Wang, Z. Jia, J. Li, et al., "Attractive Electron Delocalization Behavior of FeCoMoPB Amorphous Nanoplates for Highly Efficient Alkaline Water Oxidation," *Small* 18, no. 46 (2022): 2204135, https://doi.org/10.1002/smll.202204135.

95. F. Lyu, C. Liu, S. Zeng, et al., "Boosting Hydrogen Evolution Activity: Next-Nearest Oxygen Coordination in Dual-Phase Supra-Nanostructured Multiprincipal Element Alloy Catalysts," *Energy & Environmental Science* 17, no. 20 (2024): 7908–7918, https://doi.org/10.1039/d4ee03150d.

96. F. Lyu, S. Zeng, Z. Jia, et al., "Two-Dimensional Mineral Hydrogel-Derived Single Atoms-Anchored Heterostructures for Ultrastable Hydrogen Evolution," *Nature Communications* 13, no. 1 (2022): 6249, https://doi.org/10.1038/s41467-022-33725-8.

97. Y. Chen, J. Qiu, F. Jiang, et al., "The Integral Role of High-Entropy Alloys in Advancing Solid-State Hydrogen Storage," *Interdisciplinary Materials* 4, no. 1 (2024): 75–108, https://doi.org/10.1002/idm2.12216.

98. A. Kumar, N. K. Mukhopadhyay, and T. P. Yadav, "Hydrogen Storage in High Entropy Alloys," in *Towards Hydrogen Infrastructure: Advances and Challenges in Preparing for the Hydrogen Economy* (Elsevier Ltd., 2024), 133, https://doi.org/10.1016/b978-0-323-95553-9.00007-8.

99. A. Wetzel, M. von der Au, P. M. Dietrich, J. Radnik, O. Ozcan, and J. Witt, "The Comparison of the Corrosion Behavior of the CrCoNi Medium Entropy Alloy and CrMnFeCoNi High Entropy Alloy," *Applied Surface Science* 601 (2022): 154171, https://doi.org/10.1016/j.apsusc.2022.154171.

100. H. Ren, R. R. Chen, X. F. Gao, et al., "High-Performance AlCoCrFeNi High Entropy Alloy With Marine Application Perspective," *Journal of Materials Research and Technology* 25 (2023): 6751–6763, https://doi.org/10.1016/j.jmrt.2023.07.135.

101. W. Y. Li, M. L. Wang, X. Di Wang, T. M. Wang, T. J. Li, and Y. P. Lu, "A Novel Co-Free High-Entropy Alloy With Excellent Antimicrobial and Mechanical Properties," *Rare Metals* 44, no. 1 (2025): 581–590, https://doi.org/10.1007/s12598-024-02957-6.

102. H. Wu, T. Jiang, L. Kong, X. Chen, and P. Liu, "The Mechanical Properties, Corrosion Resistance, and Biocompatibility of a Novel Ternary Ti-*x*Nb-5Ta Alloy for Biomedical Applications," *Materials* 18, no. 3 (2025): 602, https://doi.org/10.3390/ma18030602.

103. A. R. Ahmady, A. Ekhlasi, A. Nouri, M. H. Nazarpak, P. Gong, and A. Solouk, "High Entropy Alloy Coatings for Biomedical Applications: A Review," *Smart Materials in Manufacturing* 1 (2023): 100009, https://doi.org/10.1016/j.smmf.2022.100009.

104. J. Zhu, M. Lv, C. Liu, X. Tan, and H. Xu, "Effect of Neodymium and Yttrium Addition on Microstructure and DC Soft Magnetic Property of Dual-Phase FeCoNi$(CuAl)_{0.8}$ High-Entropy Alloy," *Journal of Rare Earths* 41, no. 10 (2023): 1562–1567, https://doi.org/10.1016/j.jre.2022.06.005.

105. J. Kitagawa, "Magnetic Properties, Electrical Resistivity, and Hardness of High-Entropy Alloys FeCoNiPd and FeCoNiPt," *Journal of Magnetism and Magnetic Materials* 563 (2022): 170024, https://doi.org/10.1016/j.jmmm.2022.170024.

106. M. Y. Abdul Salam, E. N. Ogunmuyiwa, V. K. Manisa, A. Yahya, and I. A. Badruddin, "Effect of Fabrication Techniques of High Entropy Alloys: A Review With Integration of Machine Learning," *Results in Engineering* 25 (2025): 104441, https://doi.org/10.1016/j.rineng.2025.104441.

107. G. N. P. Tazuddin and K. Biswas, "In the Quest of Single Phase Multi-Component Multiprincipal High Entropy Alloys," *Journal of Alloys and Compounds* 697 (2017): 434, https://doi.org/10.1016/j.jallcom.2016.11.383.

108. T. P. C. Klaver, D. Simonovic, and M. H. F. Sluiter, "Brute Force Composition Scanning With a CALPHAD Database to Find Low Temperature Body Centered Cubic High Entropy Alloys," *Entropy* 20, no. 12 (2018): 911, https://doi.org/10.3390/e20120911.

109. Z. Li, A. Ludwig, A. Savan, H. Springer, and D. Raabe, "Combinatorial Metallurgical Synthesis and Processing of High-Entropy Alloys," *Journal of Materials Research* 33, no. 19 (2018): 3156–3169, https://doi.org/10.1557/jmr.2018.214.

110. S. Cao and J. C. Zhao, "Application of Dual-Anneal Diffusion Multiples to the Effective Study of Phase Diagrams and Phase Transformations in the Fe-Cr-Ni System," *Acta Materialia* 88 (2015): 196–206, https://doi.org/10.1016/j.actamat.2014.12.027.

111. P. Wilson, R. Field, and M. Kaufman, "The Use of Diffusion Multiples to Examine the Compositional Dependence of Phase Stability and Hardness of the Co-Cr-Fe-Mn-Ni High Entropy Alloy System," *Intermetallics* 75 (2016): 15–24, https://doi.org/10.1016/j.intermet.2016.04.007.

112. B. A. Welk, R. E. A. Williams, G. B. Viswanathan, M. A. Gibson, P. K. Liaw, and H. L. Fraser, "Nature of the Interfaces Between the Constituent Phases in the High Entropy Alloy CoCrCuFeNiAl," *Ultramicroscopy* 134 (2013): 193–199, https://doi.org/10.1016/j.ultramic.2013.06.006.

113. T. Borkar, B. Gwalani, D. Choudhuri, et al., "A Combinatorial Assessment of $Al_xCrCuFeNi_2$ ($0 < x < 1.5$) Complex Concentrated Alloys: Microstructure, Microhardness, and Magnetic Properties," *Acta Materialia* 116 (2016): 63–76, https://doi.org/10.1016/j.actamat.2016.06.025.

114. A. Marshal, K. G. Pradeep, D. Music, S. Zaefferer, P. S. De, and J. M. Schneider, "Combinatorial Synthesis of High Entropy Alloys: Introduction of a Novel, Single Phase, Body-Centered-Cubic FeMnCoCrAl Solid Solution," *Journal of Alloys and Compounds* 691 (2017): 683–689, https://doi.org/10.1016/j.jallcom.2016.08.326.

115. V. Sorkin, Z. G. Yu, S. Chen, T. L. Tan, Z. Aitken, and Y. W. Zhang, "First Principles-Based Design of Lightweight High Entropy Alloys," *Scientific Reports* 13, no. 1 (2023): 22549, https://doi.org/10.1038/s41598-023-49258-z.

116. F. Tian, D. Wang, J. Shen, and Y. Wang, "An Ab Initio Investgation of Ideal Tensile and Shear Strength of TiVNbMo High-Entropy Alloy," *Materials Letters* 166 (2016): 271–275, https://doi.org/10.1016/j.matlet.2015.12.064.

117. D. Jiang, L. Xie, and L. Wang, "Current Application Status of Multi-Scale Simulation and Machine Learning in Research on High-Entropy Alloys," *Journal of Materials Research and Technology* 26 (2023): 1341–1374, https://doi.org/10.1016/j.jmrt.2023.07.233.

118. Z. H. Aitken, V. Sorkin, and Y. W. Zhang, "Atomistic Modeling of Nanoscale Plasticity in High-Entropy Alloys," *Journal of Materials Research* 34, no. 9 (2019): 1509–1532, https://doi.org/10.1557/jmr.2019.50.

119. P. Liu, H. Zhang, Q. Hu, X. Ding, and J. Sun, "First-Principles Design of High Strength Refractory High-Entropy Alloys," *Journal of*

Materials Research and Technology 29 (2024): 3420–3436, https://doi.org/10.1016/j.jmrt.2024.02.064.

120. Z. Wang, J. Li, Q. H. Fang, B. Liu, and L. Zhang, "Investigation into Nanoscratching Mechanical Response of AlCrCuFeNi High-Entropy Alloys Using Atomic Simulations," *Applied Surface Science* 416 (2017): 470–481, https://doi.org/10.1016/j.apsusc.2017.04.009.

121. L. Li, H. Chen, Q. Fang, et al., "Effects of Temperature and Strain Rate on Plastic Deformation Mechanisms of Nanocrystalline High-Entropy Alloys," *Intermetallics* 120 (2020): 106741, https://doi.org/10.1016/j.intermet.2020.106741.

122. Y. C. Yang, C. Liu, C. Y. Lin, and Z. Xia, "The Effect of Local Atomic Configuration in High-Entropy Alloys on the Dislocation Behaviors and Mechanical Properties," *Materials Science and Engineering A* 815 (2021): 141253, https://doi.org/10.1016/j.msea.2021.141253.

123. J. Xiao and C. Deng, "Martensite Transformation Induced Superplasticity and Strengthening in Single Crystalline CoNiCrFeMn High Entropy Alloy Nanowires: A Molecular Dynamics Study," *Materials Science and Engineering A* 793 (2020): 139853, https://doi.org/10.1016/j.msea.2020.139853.

124. T. N. Vu, V. T. Pham, and T. H. Fang, "Influences of Grain Size, Temperature, and Strain Rate on Mechanical Properties of $Al_{0.3}$CoCrFeNi High–Entropy Alloys," *Materials Science and Engineering A* 858 (2022): 144158, https://doi.org/10.1016/j.msea.2022.144158.

125. S. Mooraj and W. Chen, "A Review on High-Throughput Development of High-Entropy Alloys by Combinatorial Methods," *Journal of Materials Informatics* 3, no. 1 (2023): 4, https://doi.org/10.20517/jmi.2022.41.

126. P. L. J. Conway, T. P. C. Klaver, J. Steggo, and E. Ghassemali, "High Entropy Alloys Towards Industrial Applications: High-Throughput Screening and Experimental Investigation," *Materials Science and Engineering A* 830 (2022): 142297, https://doi.org/10.1016/j.msea.2021.142297.

127. K. Guruvidyathri, K. C. Hari Kumar, J. W. Yeh, and B. S. Murty, "Topologically Close-Packed Phase Formation in High Entropy Alloys: A Review of Calphad and Experimental Results," *JOM* 69, no. 11 (2017): 2113–2124, https://doi.org/10.1007/s11837-017-2566-5.

128. J. Y. Mo, Y. X. Wan, Z. B. Zhang, et al., "First-Principle Prediction of Structural and Mechanical Properties in $NbMoTaWRe_x$ Refractory High-Entropy Alloys With Experimental Validation," *Rare Metals* 41, no. 10 (2022): 3343–3350, https://doi.org/10.1007/s12598-022-02054-6.

129. F. Tian, "A Review of Solid-Solution Models of High-Entropy Alloys Based on Ab Initio Calculations," *Frontiers in Materials* 4 (2017): 36, https://doi.org/10.3389/fmats.2017.00036.

130. H. Xie, X. Li, X. Wang, et al., "First-Principles Study on the Structure, Fracture Toughness, and Thermodynamic Properties of a New-Designed $Co_{30}Ni_{30}Fe_{20}Cr_{20}$ High-Entropy Alloy," *Journal of Materials Research and Technology* 18 (2022): 3971–3976, https://doi.org/10.1016/j.jmrt.2022.04.071.

131. K. Xiong, B. W. Wang, Z. P. Sun, et al., "Frist-Principles Prediction of Elastic, Electronic, and Thermodynamic Properties of High Entropy Carbide Ceramic (TiZrNbTa)C," *Rare Metals* 41, no. 3 (2022): 1002–1014, https://doi.org/10.1007/s12598-021-01834-w.

132. V. Sorkin, T. L. Tan, Z. G. Yu, and Y. W. Zhang, "High-Throughput Calculations Based on the Small Set of Ordered Structures Method for Non-Equimolar High Entropy Alloys," *Computational Materials Science* 188 (2021): 110213, https://doi.org/10.1016/j.commatsci.2020.110213.

133. S. Liu and C. Yang, "Machine Learning Design for High-Entropy Alloys: Models and Algorithms," *Metals* 14, no. 2 (2024): 235, https://doi.org/10.3390/met14020235.

134. G. R. Schleder, A. C. M. Padilha, C. M. Acosta, M. Costa, and A. Fazzio, "From DFT to Machine Learning: Recent Approaches to Materials Science - A Review," *Journal of Physics: Materials* 2, no. 3 (2019): 032001, https://doi.org/10.1088/2515-7639/ab084b.

135. P. Mehta, M. Bukov, C. H. Wang, et al., "A High-Bias, Low-Variance Introduction to Machine Learning for Physicists," *Physics Reports* 810 (2019): 1–124, https://doi.org/10.1016/j.physrep.2019.03.001.

136. S. Elkatatny, W. Abd-Elaziem, T. A. Sebaey, M. A. Darwish, and A. Hamada, "Machine-Learning Synergy in High-Entropy Alloys: A Review," *Journal of Materials Research and Technology* 33 (2024): 3976–3997, https://doi.org/10.1016/j.jmrt.2024.10.034.

137. H. Li, J. Wang, Q. Xu, et al., "High-Strength Medium-Entropy Alloy Designed by Precipitation-Strengthening Mechanism via Machine Learning," *Materials Science and Engineering A* 882 (2023): 145443, https://doi.org/10.1016/j.msea.2023.145443.

138. U. Bhandari, M. R. Rafi, C. Zhang, and S. Yang, "Yield Strength Prediction of High-Entropy Alloys Using Machine Learning," *Materials Today Communications* 26 (2021): 101871, https://doi.org/10.1016/j.mtcomm.2020.101871.

139. P. Raccuglia, K. C. Elbert, P. D. F. Adler, et al., "Machine-Learning-Assisted Materials Discovery Using Failed Experiments," *Nature* 533, no. 7601 (2016): 73–76, https://doi.org/10.1038/nature17439.

140. B. Meredig, A. Agrawal, S. Kirklin, et al., "Combinatorial Screening for New Materials in Unconstrained Composition Space With Machine Learning," *Physical Review B: Condensed Matter and Materials Physics* 89, no. 9 (2014): 094104, https://doi.org/10.1103/physrevb.89.094104.

141. R. Ramprasad, R. Batra, G. Pilania, A. Mannodi-Kanakkithodi, and C. Kim, "Machine Learning in Materials Informatics: Recent Applications and Prospects," *Npj Computational Materials* 3, no. 1 (2017): 54, https://doi.org/10.1038/s41524-017-0056-5.

142. G. Liu, S. Yang, and Y. Zhong, "High-Entropy Materials Design by Integrating the First-Principles Calculations and Machine Learning: A Case Study in the Al-Co-Cr-Fe-Ni System," *High Entropy Alloys & Materials* 2, no. 2 (2024): 307–320, https://doi.org/10.1007/s44210-024-00041-3.

143. J. Li, B. Xie, Q. Fang, B. Liu, Y. Liu, and P. K. Liaw, "High-Throughput Simulation Combined Machine Learning Search for Optimum Elemental Composition in Medium Entropy Alloy," *Journal of Materials Science & Technology* 68 (2021): 70–75, https://doi.org/10.1016/j.jmst.2020.08.008.

144. C. Wen, Y. Zhang, C. Wang, et al., "Machine Learning Assisted Design of High Entropy Alloys With Desired Property," *Acta Materialia* 170 (2019): 109–117, https://doi.org/10.1016/j.actamat.2019.03.010.

145. L. Zhang, K. Qian, J. Huang, M. Liu, and Y. Shibuta, "Molecular Dynamics Simulation and Machine Learning of Mechanical Response in Non-Equiatomic FeCrNiCoMn High-Entropy Alloy," *Journal of Materials Research and Technology* 13 (2021): 2043–2054, https://doi.org/10.1016/j.jmrt.2021.06.021.

146. R. Machaka, "Machine Learning-Based Prediction of Phases in High-Entropy Alloys," *Computational Materials Science* 188 (2021): 110244, https://doi.org/10.1016/j.commatsci.2020.110244.

147. N. Islam, W. Huang, and H. L. Zhuang, "Machine Learning for Phase Selection in Multi-Principal Element Alloys," *Computational Materials Science* 150 (2018): 230–235, https://doi.org/10.1016/j.commatsci.2018.04.003.

148. W. Zhu, W. Huo, S. Wang, et al., "Machine Learning-Based Hardness Prediction of High-Entropy Alloys for Laser Additive Manufacturing," *JOM* 75, no. 12 (2023): 5537–5548, https://doi.org/10.1007/s11837-023-06174-x.

149. M. Bakr, J. Syarif, and I. A. T. Hashem, "Prediction of Phase and Hardness of HEAs Based on Constituent Elements Using Machine Learning Models," *Materials Today Communications* 31 (2022): 103407, https://doi.org/10.1016/j.mtcomm.2022.103407.

150. S. P. Mishra and M. R. Rahul, "A Comparative Study and Development of a Novel Deep Learning Architecture for Accelerated Identification of Microstructure in Materials Science," *Computational Materials Science* 200 (2021): 110815, https://doi.org/10.1016/j.commatsci.2021.110815.

151. S. Guo, C. Ng, J. Lu, and C. T. Liu, "Effect of Valence Electron Concentration on Stability of fcc or bcc Phase in High Entropy Alloys," *Journal of Applied Physics* 109, no. 10 (2011): 103505, https://doi.org/10.1063/1.3587228.

152. Y. Zhang, C. Wen, C. Wang, et al., "Phase Prediction in High Entropy Alloys With a Rational Selection of Materials Descriptors and Machine Learning Models," *Acta Materialia* 185 (2020): 528–539, https://doi.org/10.1016/j.actamat.2019.11.067.

153. Z. Li, W. T. Nash, S. P. O'Brien, Y. Qiu, R. K. Gupta, and N. Birbilis, "cardiGAN: A Generative Adversarial Network Model for Design and Discovery of Multi Principal Element Alloys," *Journal of Materials Science & Technology* 125 (2022): 81–96, https://doi.org/10.1016/j.jmst.2022.03.008.

154. L. Zhang, K. Qian, B. W. Schuller, and Y. Shibuta, "Prediction on Mechanical Properties of Non-Equiatomic High-Entropy Alloy by Atomistic Simulation and Machine Learning," *Metals* 11, no. 6 (2021): 922, https://doi.org/10.3390/met11060922.

155. S. Zhao, B. Jiang, K. Song, et al., "Machine Learning Assisted Design of High-Entropy Alloys With Ultra-High Microhardness and Unexpected Low Density," *Materials & Design* 238 (2024): 112634, https://doi.org/10.1016/j.matdes.2024.112634.

156. X. Li, C. Wang, L. Zhang, et al., "Machine Learning-Based Comprehensive Prediction Model for $L1_2$ Phase-Strengthened Fe–Co–Ni-Based High-Entropy Alloys," *Acta Metallurgica Sinica* 37, no. 11 (2024): 1858–1874, https://doi.org/10.1007/s40195-024-01774-1.

157. C. Zeng, A. Neils, J. Lesko, and N. Post, "Machine Learning Accelerated Discovery of Corrosion-Resistant High-Entropy Alloys," *Computational Materials Science* 237 (2024): 112925, https://doi.org/10.1016/j.commatsci.2024.112925.

158. S. Tsopanidis and S. Osovski, "Unsupervised Machine Learning in Fractography: Evaluation and Interpretation," *Materials Characterization* 182 (2021): 111551, https://doi.org/10.1016/j.matchar.2021.111551.

159. M. Biswas, R. Pramanik, S. Sen, A. Sinitca, D. Kaplun, and R. Sarkar, "Microstructural Segmentation Using a Union of Attention Guided U-Net Models With Different Color Transformed Images," *Scientific Reports* 13, no. 1 (2023): 5737, https://doi.org/10.1038/s41598-023-32318-9.

160. Y. Li, X. Zhou, T. Colnaghi, et al., "Convolutional Neural Network-Assisted Recognition of Nanoscale $L1_2$ Ordered Structures in Face-Centred Cubic Alloys," *Npj Computational Materials* 7, no. 1 (2021): 8, https://doi.org/10.1038/s41524-020-00472-7.

161. B. L. DeCost, T. Francis, and E. A. Holm, "Exploring the Microstructure Manifold: Image Texture Representations Applied to Ultrahigh Carbon Steel Microstructures," *Acta Materialia* 133 (2017): 30–40, https://doi.org/10.1016/j.actamat.2017.05.014.

162. K. Kaufmann, C. Zhu, A. S. Rosengarten, et al., "Crystal Symmetry Determination in Electron Diffraction Using Machine Learning," *Science* 367, no. 6477 (2020): 564–568, https://doi.org/10.1126/science.aay3062.

163. B. Ma, X. Wei, C. Liu, et al., "Data Augmentation in Microscopic Images for Material Data Mining," *Npj Computational Materials* 6, no. 1 (2020): 125, https://doi.org/10.1038/s41524-020-00392-6.

164. M. Ragone, M. T. Saray, L. Long, R. Shahbazian-Yassar, F. Mashayek, and V. Yurkiv, "Deep Learning for Mapping Element Distribution of High-Entropy Alloys in Scanning Transmission Electron Microscopy Images," *Computational Materials Science* 201 (2022): 110905, https://doi.org/10.1016/j.commatsci.2021.110905.

165. Z. Pei, K. A. Rozman, ÖN. Doğan, et al., "Machine-Learning Microstructure for Inverse Material Design," *Advanced Science* 8, no. 23 (2021): 2101207, https://doi.org/10.1002/advs.202101207.

166. K. Liu, J. Wang, X. Li, Q. Qin, S. Wu, and H. Yu, "A New Lightweight $Al_{2.7}$TiVCrCu High Entropy Alloy With Excellent Strength and Toughness After Homogenization Treatment," *Materials Science and Engineering A* 869 (2023): 144779, https://doi.org/10.1016/j.msea.2023.144779.

167. M. Ghanbariha, M. Farvizi, T. Ebadzadeh, and A. Alizadeh Samiyan, "Effect of ZrO_2 Particles on the Nanomechanical Properties and Wear Behavior of AlCoCrFeNi–ZrO_2 High Entropy Alloy Composites," *Wear* 484–485 (2021): 204032, https://doi.org/10.1016/j.wear.2021.204032.

168. Z. U. Arif, M. Y. Khalid, E. ur Rehman, S. Ullah, M. Atif, and A. Tariq, "A Review on Laser Cladding of High-Entropy Alloys, Their Recent Trends and Potential Applications," *Journal of Manufacturing Processes* 68 (2021): 225–273, https://doi.org/10.1016/j.jmapro.2021.06.041.

169. X. X. Lv, W. T. Liu, J. Q. Li, et al., "High-Throughput Additive Manufacturing and Characterization of CoCrFeNi–AlTi High-Entropy Alloys," *Rare Metals* 44, no. 3 (2024): 1943–1957, https://doi.org/10.1007/s12598-024-03148-z.

170. W. J. Zhao, C. Y. Liu, P. C. Che, et al., "Microstructures and Mechanical Properties of Laser-Directed Energy Deposited CrCoNi Medium-Entropy Alloy," *Rare Metals* 43, no. 7 (2024): 3286–3300, https://doi.org/10.1007/s12598-024-02628-6.

171. A. O. Moghaddam, N. A. Shaburova, M. N. Samodurova, A. Abdollahzadeh, and E. A. Trofimov, "Additive Manufacturing of High Entropy Alloys: A Practical Review," *Journal of Materials Science & Technology* 77 (2021): 131, https://doi.org/10.1016/j.jmst.2020.11.029.

172. Y. Wu, X. Zhao, Q. Chen, et al., "Strengthening and Fracture Mechanisms of a Precipitation Hardening High-Entropy Alloy Fabricated by Selective Laser Melting," *Virtual and Physical Prototyping* 17, no. 3 (2022): 451–467, https://doi.org/10.1080/17452759.2022.2037055.

173. D. Vogiatzief, A. Evirgen, M. Pedersen, and U. Hecht, "Laser Powder Bed Fusion of an Al-Cr-Fe-Ni High-Entropy Alloy Produced by Blending of Prealloyed and Elemental Powder: Process Parameters, Microstructures and Mechanical Properties," *Journal of Alloys and Compounds* 918 (2022): 165658, https://doi.org/10.1016/j.jallcom.2022.165658.

174. D. Lin, L. Xu, X. Li, et al., "A Si-containing FeCoCrNi High-Entropy Alloy With High Strength and Ductility Synthesized In Situ via Selective Laser Melting," *Additive Manufacturing* 35 (2020): 101340, https://doi.org/10.1016/j.addma.2020.101340.

175. D. Lin, L. Xu, Y. Han, et al., "Structure and Mechanical Properties of a FeCoCrNi High-Entropy Alloy Fabricated via Selective Laser Melting," *Intermetallics* 127 (2020): 106963, https://doi.org/10.1016/j.intermet.2020.106963.

176. B. Rankouhi, S. Jahani, F. E. Pfefferkorn, and D. J. Thoma, "Compositional Grading of a 316L-Cu Multi-Material Part Using Machine Learning for the Determination of Selective Laser Melting Process Parameters," *Additive Manufacturing* 38 (2021): 101836, https://doi.org/10.1016/j.addma.2021.101836.

177. H. S. Park, D. S. Nguyen, T. Le-Hong, and X. Van Tran, "Machine Learning-Based Optimization of Process Parameters in Selective Laser Melting for Biomedical Applications," *Journal of Intelligent Manufacturing* 33, no. 6 (2022): 1843–1858, https://doi.org/10.1007/s10845-021-01773-4.

178. H. Wang, B. Li, and F. Z. Xuan, "A Dimensionally Augmented and Physics-Informed Machine Learning for Quality Prediction of Additively Manufactured High-Entropy Alloy," *Journal of Materials Processing Technology* 307 (2022): 117637, https://doi.org/10.1016/j.jmatprotec.2022.117637.

179. A. Bajpai, Z. Rao, A. Dixit, K. Biswas, and D. Raabe, "Interpretable Machine Learning for High-Strength High-Entropy Alloy Design," *arXiv Prepr arXiv240914905* (2024), http://arxiv.org/abs/2409.14905.

180. C. C. Aggarwal, *Neural Networks and Deep Learning*. 2nd ed. (Springer, 2023), 529, https://doi.org/10.1007/978-3-031-29642-0.

181. X. Liu, J. Zhang, and Z. Pei, "Machine Learning for High-Entropy Alloys: Progress, Challenges and Opportunities," *Progress in Materials Science* 131 (2023): 101018, https://doi.org/10.1016/j.pmatsci.2022.101018.

182. J. Berry, R. Snell, M. Anderson, et al., "Design and Selection of High Entropy Alloys for Hardmetal Matrix Applications Using a Coupled Machine Learning and Calculation of Phase Diagrams Methodology," *Advanced Engineering Materials* 26, no. 10 (2024): 2302064, https://doi.org/10.1002/adem.202302064.

183. S. Gao, Z. Gao, and F. Zhao, "Machine Learning and Visualization Assisted Solid Solution Strengthening Phase Prediction of High Entropy Alloys," *Materials Today Communications* 35 (2023): 105894, https://doi.org/10.1016/j.mtcomm.2023.105894.

184. H. Wang, B. Li, J. Gong, and F. Z. Xuan, "Machine Learning-Based Fatigue Life Prediction of Metal Materials: Perspectives of Physics-Informed and Data-Driven Hybrid Methods," *Engineering Fracture Mechanics* 284 (2023): 109242, https://doi.org/10.1016/j.engfracmech.2023.109242.

185. M. Q. Ha, D. N. Nguyen, V. C. Nguyen, et al., "Evidence-Based Recommender System for High-Entropy Alloys," *Nature Computational Science* 1, no. 7 (2021): 470–478, https://doi.org/10.1038/s43588-021-00097-w.

186. K. S. Vecchio, O. F. Dippo, K. R. Kaufmann, and X. Liu, "High-Throughput Rapid Experimental Alloy Development (HT-READ)," *Acta Materialia* 221 (2021): 117352, https://doi.org/10.1016/j.actamat.2021.117352.

187. T. J. Jacobsson, A. Hultqvist, A. García-Fernández, et al., "An Open-Access Database and Analysis Tool for Perovskite Solar Cells Based on the FAIR Data Principles," *Nature Energy* 7 (2022): 107–115, https://www.nature.com/articles/s41560-021-00941-3.

188. F. Zhang, K. Huang, K. Zhao, et al., "Directed Energy Deposition Combining High-Throughput Technology and Machine Learning to Investigate the Composition-Microstructure-Mechanical Property Relationships in Titanium Alloys," *Journal of Materials Processing Technology* 311 (2023): 117800, https://doi.org/10.1016/j.jmatprotec.2022.117800.